

EFFECT OF HYDROGEN ON FATIGUE BEHAVIOR OF A CADMIUM
COATED HIGH STRENGTH STEEL

A THESIS SUBMITTED TO
THE GRADUATE SCHOOL OF NATURAL AND APPLIED SCIENCES
OF
MIDDLE EAST TECHNICAL UNIVERSITY

BY

ÜMRAN BAŞAK GÜLEKEN

IN PARTIAL FULFILLMENT OF THE REQUIREMENTS
FOR
THE DEGREE OF MASTER OF SCIENCE
IN
METALLURGICAL AND MATERIALS ENGINEERING

JUNE 2019

Approval of the thesis:

**EFFECT OF HYDROGEN ON FATIGUE BEHAVIOR OF A CADMIUM
COATED HIGH STRENGTH STEEL**

submitted by **ÜMRAN BAŞAK GÜLEKEN** in partial fulfillment of the requirements for the degree of **Master of Science in Metallurgical and Materials Engineering Department, Middle East Technical University** by,

Prof. Dr. Halil Kalıpçılar
Dean, Graduate School of **Natural and Applied Sciences**

Prof. Dr. C. Hakan Gür
Head of Department, **Met. and Mat. Eng.**

Prof. Dr. Rıza Gürbüz
Supervisor, **Met. and Mat. Eng., METU**

Prof. Dr. Bilgehan Ögel
Co-Supervisor, **Met. and Mat. Eng / METU**

Examining Committee Members:

Prof. Dr. Ali Kalkanlı
Met. and Mat. Eng., METU

Prof. Dr. Rıza Gürbüz
Met. and Mat. Eng., METU

Prof. Dr. Bilgehan Ögel
Met. and Mat. Eng., METU

Prof. Dr. Caner Durucan
Met. and Mat. Eng., METU

Assoc. Prof. Dr. Derya Dışpınar
Met. and Mat. Eng., İTÜ

Date: 20.06.2019

I hereby declare that all information in this document has been obtained and presented in accordance with academic rules and ethical conduct. I also declare that, as required by these rules and conduct, I have fully cited and referenced all material and results that are not original to this work.

Name, Surname: Ümran Başak Güleken

Signature:

ABSTRACT

EFFECT OF HYDROGEN ON FATIGUE BEHAVIOR OF A CADMIUM COATED HIGH STRENGTH STEEL

Güleken, Ümran Başak
Master of Science, Metallurgical and Materials Engineering
Supervisor: Prof. Dr. Rıza Gürbüz
Co-Supervisor: Prof. Dr. Bilgehan Ögel

June 2019, 84 pages

Despite the associated health and safety concerns of Cadmium, this material remains the most commonly used fastener plating material in aerospace applications. The plating operation is done by a well understood and common electrodeposition process. If a cadmium plated part has high strength (1000 MPa and above) then in order to prevent hydrogen embrittlement it must be baked at 191°C for 23 hours, within 2 hours after plating. Yet it has been seen that parts fail due to hydrogen embrittlement during service. The first stage of this study investigated the potential for an 8-hour test (developed by Drehler) instead of the aerospace industry standard 200-hour test (QQ – P – 416). The second phase involved an investigation into the effect of hydrogen on crack initiation-based fatigue life of a modified 4340 steel, utilising a rotating beam fatigue test and presenting data within S – N curves. A batch of as-coated samples and a batch of preloaded samples were fatigue tested by rotating beam testing machine. Although the 8-hour test results indicated possible hydrogen absorption, the fatigue test results showed minimal variation in fatigue performance. The most distinctive detrimental change in fatigue behaviour was observed within preloaded samples. Prediction of the mechanisms leading to premature failure of aerospace components was the ultimate purpose of this work.

Keywords: AISI 4340 Steel, Cadmium Coating, Hydrogen Embrittlement, 8-Hour (Step Load) Test, Crack Initiation Based Fatigue Life

ÖZ

KADMIYUM KAPLANMIŞ YÜKSEK MUKAVEMETLİ BİR ÇELİKTE HİDROJENİN YORULMA DAVRANIŞINA ETKİLERİ

Güleken, Ümran Başak
Yüksek Lisans, Metalurji ve Malzeme Mühendisliği
Tez Danışmanı: Prof. Dr. Rıza Gürbüz
Ortak Tez Danışmanı: Prof. Dr. Bilgehan Ögel

Haziran 2019, 84 sayfa

Kadmiyum sağlık açısından zararlarına rağmen hala havacılık uygulamalarında kullanılan ve cıvata bileşenlerinde kullanılan en yaygın kaplama malzemesidir. Kaplama, oldukça yaygın ve iyi anlaşılmış bir proses olan elektro birikim yöntemiyle gerçekleştirilir. Yüksek mukavemetli çeliklerde (1000 MPA ve üzeri) hidrojen gevrekliğini önlemek için kadmiyum kaplamadan sonra malzemenin, kaplamayı takip eden 2 saat içerisinde, 191°C 'de 23 saat boyunca fırınlanması gerekmektedir. Buna rağmen parçaların hizmet süreleri içerisinde hidrojen gevrekliği sebebiyle hasarlanabildiği gözlemlenmektedir. Bu çalışmanın ilk aşaması, havacılık endüstrisinde en yaygın kullanıma sahip standart olan QQ – P – 416'da tariflenen 200 saat testi yerine Drehler tarafından geliştirilmiş olan 8 saat testinin kullanılıp kullanılmayacağını belirlemektir. İkinci aşamada ise modifiye edilmiş bir 4340 çeliğinde yorulma çatlak oluşumu tabanlı yorulma ömrü üzerinde hidrojenin etkilerini dönen çubuk yorulma testi aracılığıyla elde edilen verilerle oluşturulan S – N eğrileri oluşturulmuştur. Dönen çubuk yorulma testinde ön yükleme yapılmamış ve ön yükleme yapılmış iki parti üzerinde çalışılmıştır. Her ne kadar 8 saat testi sonuçları hidrojen emilimi ihtimalini belirttiyse de test sonuçları kullanılarak elde edilen S – N eğrilerinde yorulma ömrü davranışında sadece ufak değişiklikler gözlemlenmiştir.

Yorulma ömründe en dikkat çekici olumsuz deęişim ön yükleme uygulanan numunelerden alınan sonuçlarda gözlemlenmiştir. Nihai amaç ise havacılık endüstrisinde kullanılan bileşenlerin erken hasarlanmasına sebep olan mekanizmayı öngörmektir.

Anahtar Kelimeler: AISI 4340 Çelięi, Kadmiyum Kaplama, Hidrojen Gevreklięi, 8 Saat (Aşamalı Yükleme) Testi, Çatlak Başlangıcı Tabanlı Yorulma Ömrü

To My Precious Family

ACKNOWLEDGEMENTS

I should like to thank Prof. Dr. Rıza Gürbüz and Prof. Dr. Bilgehan Ögel for their encouragement, guidance and support.

I should also like to thank my dear friends Volkan Kartal, Tufan Güngören, Zeren Taşkaya, Fatih Altunköseođlu, Ela Küçük and Aslıhan Tokat for their patience and support.

The technical assistance of my lab mate Mr. Ali Motameni Tabatabaei, technicians Mr. Cemal Yanardağ, Mr. Servet Şehirli and Mr. Önder Şahin were remarkable.

Special thanks must also go to 5th Main Maintenance Centre for its cooperation and the use of its facilities; without its support this study would never been possible.

I cannot emphasize enough the impotence the love and support of my family has been throughout my Masters journey, particularly my dear grandmother Bahtısen Altan, my sister Aslı Güleken, my mother Hatice Fügen Güleken and especially my father Ali Ömer Güleken. Their support and acceptance from the first day of my work, has been relentless and hugely appreciated.

Last but not least, I should also like to thank my aunt Fatma Güler Biner and my cousins Zerrin Özlem Biner and Zahide Özge Biner for being there whenever I needed.

Finally, I should like to dedicate my success to the memory of my grandparents Mehmet Fahri Altan, Ümran Güleken and Major General Mehmet Reşat Güleken.

TABLE OF CONTENTS

ABSTRACT.....	v
ÖZ.....	vii
ACKNOWLEDGEMENTS	x
TABLE OF CONTENTS.....	xi
LIST OF TABLES	xiv
LIST OF FIGURES	xvi
CHAPTERS	
1. INTRODUCTION	1
2. LITERATURE REVIEW	3
2.1. 4XXX Series and Grade 4340	3
2.1.1. Heat Treatment of AISI 4340 Steel	6
2.1.1.1. Annealing	6
2.1.1.2. Normalizing.....	6
2.1.1.3. Hardening	7
2.1.1.4. Tempering	7
2.1.2. Machinability and Welding	8
2.1.2.1. Machinability	8
2.1.2.2. Welding.....	8

2.2. Cadmium Coating and Its Use in Aerospace Applications.....	8
2.2.1. Industrial Processes to Deposit Cadmium on Metal	10
2.2.1.1. Electroplating.....	10
2.2.1.2. Mechanical Plating	11
2.2.1.3. Vacuum and Ion Deposition	11
2.3. Hydrogen Embrittlement Phenomenon and Its Relation to Cadmium Coating Process	12
2.3.1. Industrial Trends in Testing Methods for Hydrogen Content Determination: 200 Hour Test vs 8 Hour Test	20
2.4. Determination of Fatigue Behavior Using S – N Curves and the Effect of Hydrogen.....	21
3. EXPERIMENTAL PROCEDURE.....	29
3.1. Material Used for the Experiments	29
3.2. Heat Treatment of the Base Metal	30
3.3. Directions of the Samples Used in the Experiments.....	32
3.4. Characterization of the Modified 4340 Steel Used in this Study.....	33
3.4.1. Metallography	33
3.4.2. Hardness Testing	33
3.4.3. Tensile Testing	33
3.5. Coating Process.....	34
3.6. 8-Hour Test	35
3.7. Rotating Beam Fatigue Test.....	37
4. RESULTS AND DISCUSSION	41
4.1. Microstructural Analysis.....	41
4.2. Hardness Measurements	42

4.3. Tensile Properties	42
4.4. Properties of the Coating	43
4.4.1. Coating Thickness.....	43
4.4.2. SEM Images of the Coated Layer.....	44
4.4.3. EDS Analysis of the Coated Layer	45
4.5. 8-Hour Test Results	47
4.6. Fatigue Test Results	58
5. CONCLUSION.....	79
REFERENCES.....	81

LIST OF TABLES

TABLES

Table 2.1. Designations used for major classifications of steel.....	4
Table 2.2. Summary of various properties of commercial AISI 4340 steel [1].....	5
Table 2.3. Embrittlement index comparison of AISI 4340 and 300m after application of the given coating [13].....	18
Table 3.1. Standard chemical composition of AISI 4340 steel	29
Table 3.2. Spectral analysis of the billet used to extract test samples used in this study	30
Table 3.3. Etching and coating parameters.....	35
Table 3.4. Loads used for the 8-hour test	36
Table 3.5. Dimensions of the notched tensile specimen in conformity with ASTM E8	36
Table 3.6. Conditions selected for rotating beam fatigue testing	37
Table 4.1. Brinell Hardness measurement results related to points specified at Figure 4.2	42
Table 4.2. Tensile test results	43
Table 4.3. Coating thicknesses that resulted from given etching and plating parameters	44
Table 4.4. Distribution of chromium and cadmium close to the surface.....	47
Table 4.5. Mechanical data obtained from the 8-hour test of uncoated and notched round specimen	48
Table 4.6. Summary of results of 8-hour load test composed of cycles to break and load at break.....	50
Table 4.7. Mechanical data obtained from the 8-hour test of notched round specimen 1 (2 – 4).....	51

Table 4.8. Mechanical data obtained from the 8-hour test of notched round specimen 2 (2 – 8).....	53
Table 4.9. Mechanical data obtained from the 8-hour test of notched round specimen 3 (4 – 4).....	54
Table 4.10. Mechanical data obtained from the 8-hour test of notched round specimen 4 (4 – 8).....	56
Table 4.11. Etching and coating conditions of the samples used for rotating beam fatigue testing.....	58
Table 4.12. The cycles to break data obtained from the rotating beam fatigue testing of samples in as coated condition. (No preloading) UTS% is the corresponding percentage of ultimate tensile strength of modified 4340, S is the MPa value of UTS%, F is the applied load.....	60
Table 4.13. The cycles to break data obtained from the rotating beam fatigue testing of samples that are subjected to a preloading operation before the test. UTS% is the corresponding percentage of ultimate tensile strength of modified 4340, S is the MPa value of UTS%, F is the applied load.....	62
Table 4.14. Weibull modulus of the rotating beam fatigue test results for each condition.....	67

LIST OF FIGURES

FIGURES

Figure 2.1. Hydrogen bubble migration to grain boundaries and formation of bubbles along these sites [13]	13
Figure 2.2. Hydrogen uptake from (a) Gaseous Environment and from (b) Aquatic Environment [14].....	14
Figure 2.3. Diffusion coefficient of hydrogen in ferrite and diffusion coefficient of hydrogen in austenite. diffusion occurring in ferrite with strong traps is represented by the dashed region. hydrogen's diffusivity in nickel, cadmium and tin at ambient temperature is also represented [13]	17
Figure 2.4. (a) Permeation rate of hydrogen to uncoated steel vs steel coated with 6µm cadmium (b) comparison of hydrogen evaluation rates under same conditions given in (a).....	19
Figure 2.5. The change in fracture stresses of a high strength (1516 MPa) steel alloyed with nickel, chromium, molybdenum that is electrically charged with hydrogen over time after hydrogen charging	20
Figure 2.6. Sample S – N curves of two different materials, behavior of material A shows an endurance limit whereas material B does not exhibit an endurance limit [18]	24
Figure 2.7. Graphical representation of the Basquin Slope	25
Figure 3.1. Heat treatment cycles that the modified 4340 steel used in experiments undergo (process parameters are supplied by the source manufacturer of the material)	31
Figure 3.2. Setup used by the entity that manufactured the modified 4340 steel for the water quenching operation.....	32
Figure 3.3. Representation of the modified 4340 billet and sample directions	33

Figure 3.4. Schematic representation of cadmium coating process. Each step is followed by a washing (cold rinse) operation to prevent contamination of the baths and inhibit complications like over etching.	34
Figure 3.5. Dimensions of the gauge section of the notched specimen used in the 8-hour tests	35
Figure 3.6. Two sets of identical cadmium coated, notched tensile specimens and sections cut to measure thickness molded into Bakelite. Etching and coating parameters are given in Table 3.3	37
Figure 3.7. Rotating beam testing machine (a) general appearance (b) closer look to the rotating end and the load cell above the fixture (c) data screen.....	38
Figure 3.8. Rotating beam fatigue specimen, technical drawing and the actual sample	39
Figure 4.1. SEM images of the microstructure taken from samples cut from x, y and z directions under 3,000x magnification. First column is the general appearance, some inclusions can be seen on 2 nd and 3 rd columns.....	41
Figure 4.2. Hardness measurement points and the actual section used for these measurements.....	42
Figure 4.3. The coating thicknesses measured under SEM	43
Figure 4.4. SEM images of the electrodeposited cadmium layer. (a) Top row is the appearance of the surface of the coating, (b) second row the cross section can be seen and (c) a closer view to the coating inner structure is given on the third row	45
Figure 4.5. EDS spectra of the coating layer from the middle of the coating thickness	46
Figure 4.6. EDS spectra of the coating close to the passivated surface	46
Figure 4.7. Time vs Tensile Stress graph of uncoated and notched, round tensile specimen made of modified 4340 steel subjected to 8-hour test. Sample finished the test and met the criteria so it is accepted that no hydrogen is present in the structure	47
Figure 4.8. Stress vs Strain curve obtained from the 8-hour test of uncoated and notched, round tensile specimen made of modified 4340 steel	48

Figure 4.9. SEM image of the fracture surface of uncoated specimen subjected to 8-hour test taken from the core (magnification 20,000x) 49

Figure 4.10. SEM image of the fracture surface of uncoated specimen subjected to 8-hour test taken from the modified 4340 steel and cadmium coating interface (magnification 1,025x) 49

Figure 4.11. Time vs Tensile Stress graph of notched, round tensile specimen 1 (2 – 4), made of modified 4340 steel subjected to 8-hour test, break at 4th cycle..... 50

Figure 4.12. Stress vs Strain curve obtained from the 8-hour test of notched, round tensile specimen 1 (2 – 4) 51

Figure 4.13. Time vs Tensile Stress graph of notched, round tensile specimen 2 (2 – 8), made of modified 4340 steel subjected to 8-hour test, break at 3rd cycle 52

Figure 4.14. Stress vs Strain curve obtained from the 8-hour test of notched, round tensile specimen 2 (2 – 8) 52

Figure 4.15. Time vs Tensile Stress graph of notched, round tensile specimen 3 (4 – 4), made of modified 4340 steel subjected to 8-hour test, break at 4th cycle..... 53

Figure 4.16. Stress vs Strain curve obtained from the 8-hour test of notched, round tensile specimen 3 (4 – 4) 54

Figure 4.17. Time vs Tensile Stress graph of notched, round tensile specimen 4 (4 – 8), made of modified 4340 steel subjected to 8-hour test, break at 3rd cycle 55

Figure 4.18. Stress vs Strain curve obtained from the 8-hour test of notched, round tensile specimen 4 (4 – 8) 55

Figure 4.19. SEM image of the fracture surface of specimen 1 (2 – 4) subjected to 8-hour test taken from the core of the sample (on the left) modified 4340 steel and cadmium coating interface (on the right)..... 56

Figure 4.20. SEM image of the fracture surface of specimen 2 (2 – 8), 3 (4 – 4) and 4 (4 – 8), respectively, all after being subjected to 8-hour test. Photos are taken from (a) the core of the sample and (b) from the modified 4340 steel and cadmium coating interface 57

Figure 4.21. Some interesting features at fracture surface of 3rd specimen (4 – 4) located near the modified 4340 steel and cadmium coating interface..... 57

Figure 4.22. The semi log plot of S vs N for uncoated, 4 min etched 8 min coated (4 – 8), 4 min etched 4 min coated (4 – 4), 2 min etched 8 min coated (2 – 8) samples using data tabulated in Table 4.12	61
Figure 4.23. The semi log plot of S vs N for uncoated, preloaded samples of 4 min etched 8 min coated (P4 – 8) condition, preloaded samples of 4 min etched 4 min coated (P4 – 4) condition and samples of 2 min etched 8 min coated (2 – 8) condition using data tabulated in Table 4.13	62
Figure 4.24. Comparison of S – N curves belonging to uncoated samples, unloaded (4 – 8) and preloaded (P4 – 8) samples of 4 min etching 8 min coating condition.....	63
Figure 4.25. Comparison of S – N curves belonging to uncoated samples, unloaded (4 – 4) and preloaded (P4 – 4) samples of 4 min etching 4 min coating condition.....	64
Figure 4.26. Comparison of S – N curves belonging to uncoated samples, unloaded (2 – 8) and preloaded (P2 – 8) samples of 2 min etching 8 min coating condition.....	65
Figure 4.27. Weibull distribution of uncoated samples and samples without preloading	66
Figure 4.28. Weibull distribution of uncoated samples and samples with preloading	66
Figure 4.29. Graphical representation of Weibull modulus of S – N data collected from all coating and loading conditions.....	67
Figure 4.30. Graphical representation of the Basquin slope along with related equations for uncoated sample and unloaded samples.....	68
Figure 4.31. Graphical representation of the Basquin slope along with related equations for uncoated sample and preloaded samples.....	68
Figure 4.32. Macro images of the fracture surfaces of uncoated samples after the rotating beam fatigue test	69
Figure 4.33. SEM images of possible crack initiation point and typical fatigue marks observed on the fracture surface of uncoated sample subjected to cyclic loading under 140 N.....	69

Figure 4.34. SEM images of possible crack initiation point and typical fatigue marks observed on the fracture surface of uncoated sample subjected to cyclic loading under 350 N. 70

Figure 4.35. SEM images of a representative area where crack propagation can be observed on the fracture surface of uncoated sample subjected to cyclic loading under 350 N 70

Figure 4.36. SEM image of fast fracture are ductile nature is observed on the fracture surface of uncoated sample subjected to cyclic loading under 350 N..... 71

Figure 4.37. Macro images of the fracture surfaces of the samples that were coated under given conditions after the rotating beam fatigue test. No load was introduced prior to fatigue testing..... 71

Figure 4.38. Image from the Sample (2 – 8) fractured under cyclic loading of 140 N showing (a) crack propagation at center and (b) possible fast fracture area at the edge 72

Figure 4.39. Image from the Sample (2 – 8) fractured under cyclic loading of 350 N showing (a) crack initiation and (b) crack propagation 72

Figure 4.40. Image from Sample (4 – 4) fractured under cyclic loading of 140 N showing (a) crack initiation propagation and (b) crack propagation 73

Figure 4.41. Image from Sample (4 – 4) fractured under cyclic loading of 350 N showing (a) small fatigue cracks and (b) representative fatigue area..... 73

Figure 4.42. Image from the Sample (4 – 8) fractured under cyclic loading of 140 N showing (a) crack initiation and (b) crack propagation 74

Figure 4.43. Image from the Sample (4 – 8) fractured under cyclic loading of 350 N showing river patterns at the fatigue surface 74

Figure 4.44. Macro images of the fracture surfaces of the samples that were coated under given conditions after the rotating beam fatigue test. The samples were preloaded prior to fatigue testing 75

Figure 4.45. SEM images of possible crack propagation areas (a) close to edge and (b) from the centre observed on the fracture surface of preloaded sample (P2 – 8) subjected to cyclic loading under 140 N..... 75

Figure 4.46. Image from the Sample (P2 – 8) fractured under cyclic loading of 350 N
(a) sudden fracture area and (b) an area with intergranular fracture like appearance 76

Figure 4.47. Image from the Sample (P4 – 4) fractured under cyclic loading of 350 N
(a) sudden fracture area and (b) an area with intergranular fracture like appearance 76

Figure 4.48. SEM images of (a) possible crack initiation point and (b) striation marks
and crack propagation from the center observed on the fracture surface of preloaded
sample (P4 – 8) subjected to cyclic loading under 140 N.....77

Figure 4.49. Image from the Sample (P4 – 8) fractured under cyclic loading of 350 N
(a) close up of a fatigue crack and (b) typical propagation surface77

CHAPTER 1

INTRODUCTION

Although cadmium is highly toxic it is essential for aerospace industry due to its corrosion and lubrication properties. Cadmium is sacrificial when in contact with many metals. It is also compatible with high strength steels and aluminum alloys. It's toxic properties are well known but there are no replacive coatings in use yet.

It is observed that most of the premature failings of cadmium coated nuts and bolts used in helicopters are due to hydrogen embrittlement. The aim of this study is to determine whether there is a hydrogen uptake during pickling or cadmium coating stages and to understand the effect of this hydrogen on fatigue behavior of the high strength steels or AISI 4340 in particular for this study.

The aim of this study was to determine the effect of hydrogen uptake on fatigue behavior of a modified AISI 4340 steel by using 8 – hour test to predict the presence of hydrogen than measure the fatigue behavior by rotating beam fatigue test. Coating thickness was determined by SEM imaging. Different pickling and coating parameters were used to intentionally trap hydrogen in the structure.

AISI 4340 is a low alloy steel. It is heat treatable and contains chromium, nickel and molybdenum as alloying elements. It gains high toughness and high strength via heat treatment. All conventional techniques can be used to machine annealed or tempered and normalized AISI 4340 steel. In the annealed condition it has good ductility and formability. It is suitable for fusion or resistance welding. AISI 4340 steel can be forged, cold worked and hardened. Beside these properties it is also cost effective so it is a very suitable material for aeronautical applications. The base metal used for this study is a modified version that was manufactured for a classified application and the

aim was to create a structure that has superior toughness and tensile properties compared to commercial AISI 4340 grade.

Cadmium is the most common fastener plating material used at aerospace applications. Cadmium is highly toxic so the industry is under great pressure against usage of cadmium but a replacement with compatible protection is yet not available. The most common method for cadmium plating is electro deposition and the coating are comparatively easy to accomplish. On the other hand, in order to prevent hydrogen embrittlement; cadmium plated parts shall be baked at 191°C for 23 hours, within 2 hours after plating.

Melting point of cadmium is 316 °C so 232 °C is its useful service temperature limit. When use of sacrificial metallic coatings is selected as the corrosion protection method for a high strength steel there is an increased risk of failure by hydrogen embrittlement. When electrodeposition is the selected method for application of the coating the hydrogen produced by a small proportion of the plating current is reversibly trapped in the coating and then the coated steel slowly absorbs this hydrogen. Under load this hydrogen can lead to a phenomenon called delayed failure in the coated high strength steels. Failure that is tied to the possible hydrogen uptake during electroplating is called as direct embrittlement.

In this study the samples were intentionally not baked with a will to trap hydrogen in the structure. Then the presence of hydrogen was evaluated by pass or fail test referred to as 8-hour test and the S – N curves created by the results of rotating beam testing were presented along with some SEM images of the fracture surfaces.

CHAPTER 2

LITERATURE REVIEW

2.1. 4XXX Series and Grade 4340

SAE steel grades are designated by The Society of Automotive Engineers (SAE). [1] Nomenclature used by SAE is composed of four-digit numbers. These numbers stand for the chemical composition standards for the specified steel. First a very similar naming methodology was created by the American Iron and Steel Institute (AISI). AISI and SAE systems both use the same numbers to indicate the same alloy. AISI system later evolved into a system where steel making process was denoted by a letter prefix. For example, when the production method would involve the use of basic oxygen furnace, electric arc furnace or open-hearth furnace than the related steel would get "C" as a prefix or, involvement of electric arc furnace at the steel making would be indicated by the use of prefix "E" etc...

AISI involvement was stopped after 1995 as this institution never wrote any of the specifications.

In SAE system is composed of a number having four digits. In this four-digit number the main alloying element(s) are indicated by the first digit, the secondary alloying element(s) are indicated by the second digit and the amount of carbon is indicated by the last two digits. These last two digits resemble the weight percent of carbon in hundredths when the material in question is a carbon steel or an alloy steel. Say, a plain-carbon steel with 0.60 weight percent carbon would be referred to as 1060 steel.

When hardenability is to be indicated any designation can get the suffix "H". When suffix "H" is used hardenability becomes the major concern so the requirements regarding chemical composition are loosened. The hardenability becomes the defining property and this property is defined by the results of a Jominy test.

Table 2.1. Designations used for major classifications of steel

Designation	Type
1XXX	Carbon steels
2XXX	Nickel steels
3XXX	Nickel-chromium steels
4XXX	Molybdenum steels
5XXX	Chromium steels
6XXX	Chromium-vanadium steels
7XXX	Tungsten steels
8XXX	Nickel-chromium-vanadium steels
9XXX	Silicon-manganese steels

As indicated above 4XXX refers to the series of steels where molybdenum is the main alloying element. Common examples of these series can be seen below:

Molybdenum steels

40xx Mo 0.20% or 0.25% or 0.25% Mo & 0.042 S

44xx Mo 0.40% or 0.52%

Chromium-molybdenum (Chromoly) steels

41xx Cr 0.50% or 0.80% or 0.95%, Mo 0.12% or 0.20% or 0.25% or 0.30%

Nickel-chromium-molybdenum steels

43xx Ni 1.82%, Cr 0.50% to 0.80%, Mo 0.25%

43BVxx Ni 1.82%, Cr 0.50%, Mo 0.12% or 0.35%, V 0.03% min

47xx Ni 1.05%, Cr 0.45%, Mo 0.20% or 0.35%

Nickel-molybdenum steels

46xx Ni 0.85% or 1.82%, Mo 0.20% or 0.25%

48xx Ni 3.50%, Mo 0.25%

The Grade used in this study is referred to as AISI 4340. Note that the actual based metal used is a slight modification to this grade. AISI 4340 is an alloy that is referred to as Nickel-chromium-molybdenum steel. Several different designations that are used for the same grade are DIN 1.6565 (Germany); JIS SNCM 8 (Japan); B.S. 2 S 119, B.S. 3 S 95, B.S. 3111 Type 6, B.S. 817 M 40 (United Kingdom); AMS 5331, AMS 6359, AMS 6359B, AMS 6414, AMS 6414A, AMS 6415, AMS 6415G, ASTM A322, ASTM A331, ASTM A505, ASTM A519, ASTM A547, ASTM A646, MIL SPEC MIL-S-16974, SAE J404, SAE J412, SAE J770, UNS G43400 (United States)

Various expected properties of AISI 4340 can be seen in the Table 2.2 given below:

Table 2.2. Summary of various properties of commercial AISI 4340 steel [1]

PROPERTIES		CONDITIONS	
		T (°C)	TREATMENT
Density (x1000 kg/m ³)	7.7 – 8.03	25	
Poisson's Ratio	0.27 – 0.30	25	
Elastic Modulus (GPa)	190 - 210	25	
Tensile Strength (MPa)	744.6	25	Annealed at 810°C
Yield Strength (MPa)	472.3		
Elongation (%)	22.0		
Reduction in Area (%)	49.9		
Hardness (HB)	217	25	Annealed at 810°C
Impact Strength (J) (Izod)	51.1	25	Annealed at 810°C
Thermal Expansion (10 ⁻⁶ /°C)	11.5	20 - 100	Oil Hardened Tempered at 630°C
Electrical Resistivity (10 ⁻⁹ Ω – m)	248	20	

Being a low alloy heat treatable steel AISI 4340 has a wide range of applications on military and commercial aircrafts, automotive systems, machine tool and hydraulic tool applications and crankshafts. As AISI 4340 has an increased durability, use of

this grade at gun parts automotive transmission gears and craft aircraft landing gear are very frequent. The common requirement of all these parts is that they all must withstand high pressures and work well under repeated stresses

2.1.1. Heat Treatment of AISI 4340 Steel

It is necessary to heat treat this grade to arrange the machinability of the steel in question and to obtain desired mechanical properties specific to the application. Given below heat treatment processes can be applied to AISI 4340 steels for mentioned below purposes. Although some specific temperatures are given below only through practice can the optimum temperature and conditions be defined. [2]

2.1.1.1. Annealing

Annealing process for AISI 4340 is normally carried out as follows. First step is the annealing at 830°C nominal temperature, followed by cooling to 730°C and then furnace cooling at a rate of 11°C per hour to 610°C followed by air cooling. This procedure is referred to as full annealing. The aim of this treatment is to achieve a pearlitic microstructure. During this process from the austenitizing temperature to a temperature below the temperature that the transformation would be complete slow cooling shall be involved so it is a very time-consuming treatment.

If a spheroidized structure in AISI 4340 grade is desired a sample austenitization procedure is as follows. Annealing shall be carried out at 750°C, then the temperature shall be decreased to 705°C by furnace cooling followed by cooling at a rate of 3°C per hour to 565°C. The structure achieved by application of this procedure will probably have better machinability compared to the expected outcome of the full annealing process being the pearlitic structure where the perlite is formed in coarse lamellar form.

2.1.1.2. Normalizing

If a steel is heated to a temperature that is above the ferrite to austenite transformation temperature followed by air cooling to a temperature well below this ferrite to

austenite transformation temperature of this steel in question this operation is called Normalizing. Normalizing can be used before the final heat treatment procedure to condition the steel. This process is also used as a means to refine the structure of the steel. 815°C, is the generally used as the normalizing temperature for AISI 4340 grades but temperatures in the range of $\pm 10^\circ\text{C}$ around this temperature may be used depending on the previous experiences of the applicator. If normalizing would be followed by another operation like, hardening and tempering or carburizing it is a common practice to use the upper range of normalizing temperatures. Normalizing can sometimes be the final heat treatment. If this is the situation than lower temperature range is used.

2.1.1.3. Hardening

Hardening is a metalworking process and when the hardened material is AISI 4340 steel then if it is followed by quenching martensite is formed. There is generally a correlation between hardness and tensile strength. Martensite formation results in an increase in hardness and tensile strength properties of the steel. The generally accepted austenitizing temperature for direct hardening of AISI 4340 grade is between 815°C to 845 ° C. As the AISI 4340 alloy's hardenability profile is suitable for the use of oil quenching method to be applied for hardening.

2.1.1.4. Tempering

Hardening process will create internal stresses and a procedure called Tempering is carried out to relieve these internal stresses, and also to achieve the mechanical properties desired for the application that is aimed. It is not possible to give a reference temperature for this process. The tempering temperature is determined according to aimed properties. The actual temperature for tempering is chosen to meet these properties required for the application in question. Determination of the specific temperature to be used for tempering is usually done by trial and error method.

It is important to note that nitriding, flame or induction hardening can also be used.

2.1.2. Machinability and Welding

2.1.2.1. Machinability

AISI 4340 is commonly used for applications requiring heavy sections. Both the coarse lamellar pearlitic structure and spheroidized structure are readily machinable and the choice depends upon section size, complexity and the extent of machining requirements. When any other structure's suitability is something to be doubted, the heat treatment shall aim for a spheroidized structure.

2.1.2.2. Welding

In annealed condition AISI 4340 is readily welded whereas welding operations shall be avoided after hardening and tempering as they will affect the mechanical properties. If the material in question is in the nitrided, induction hardened or flame hardened conditions then welding is not a recommended operation.

For welding of this grade electrodes with low-hydrogen shall be used and the material shall be preheated between the 200 – 300°C range and this temperature should be maintained throughout the process whenever possible. Welding operation shall be followed by slow cooling in ashes or sand which shall be followed by a stress relieved operation if possible.

2.2. Cadmium Coating and Its Use in Aerospace Applications

Cadmium deposition is a method of coating applied on steel products and iron. It has wide use as a tool to provide corrosion protection, especially on steel structural components and threaded assemblies. Note that the necessary measures shall be taken to prevent hydrogen uptake during the coating process itself to avoid premature failure. Unfortunately, cadmium is highly toxic material. It causes both environmental and health problems. Due to these problems arising from its use this application become a very serious concern. Although it is banned to be used in most of the industries there is a limited allowance of its use on certain industries such as those

involving aeronautical applications as a compatible replacement coating is not yet available. [3]

Steel, aluminum, iron and brass are materials on which cadmium coatings generally are applied. [4] The coating results in excellent corrosion resistance in almost every condition with a limited number of exceptions. This especially applies to aquatic settings in alkaline and marine environments. Protection provided by cadmium is sacrificial protection just like zinc. Sacrificial protection is where even if damage to the coating occurs the and small areas of substrate such as steel is exposed the preferentially corroded material still is the remaining coating but not the substrate. This is not the only advantage obtained by this application. Cadmium coatings also provide a coefficient of friction that is low which means lubricity is good, their torque characteristics are predictable, they promote low levels of electrical resistance that results in good electrical conductivity, and they supply protection from galvanic corrosion especially when in contact with aluminum. Easy solderability like tin is another property and their corrosion products are low in volume which reduces some risks like operating mechanism's jamming by debris formed as a corrosion product on any of the components and the deposit may be classified as ductile. If used as coated exhibits extraordinary white luster identical to that of silver plating.

These properties make cadmium coatings useful in various industries such as defense, offshore, aerospace, automotive, mining, electrical and electronic industries. Cadmium coatings are commonly applied to bolts and other fasteners along with other components which include but not limited to chassis and connectors.

Apart from steel cadmium electrodeposition can also be applied on nickel, brass, aluminum, copper, beryllium copper and parts manufactured by powder metallurgy.

The resulting cadmium coating can have different thicknesses generally ranging between 5 μm and 25 μm . This can be the as coated thickness or thickness after the application of supplementary finishes. Selection of the required thickness is depending on the severity of the atmosphere that the end product will be subjected to.

Corrosion resistance is achieved by application of cadmium coatings and also base metal corrosion is prevented. [5] The as coated condition supplies protection with the lowest cost and is suitable for applications to be subjected to a non-corrosive environment or a mild environment where the function of the part in question is not threatened or effected by the corrosion products of white appearance. A supplementary finish like most commonly used chromate is applied on the cadmium coating to enhance the resistance to corrosion.

This chromate supplementary finish slows down or inhibits the formation of mentioned above corrosion products during service where the component in question is exposed to different environments. This finish also keeps the appearance of the base metal in a condition closer to the appearance right after the application.

Especially in the aerospace industry cadmium coatings are used mainly as a means of minimizing the bi-metallic corrosion. This kind of corrosion is seen between fasteners made of high-strength steel and other components made from aluminum and alloys. [6] Coefficient of friction value of the cadmium coating is comparatively low so it is not necessary to undercut the threads on fastener parts. This property makes assembly and disassembly of suggested structures numerous times. It also reduces the requirement of tightening torque.

2.2.1. Industrial Processes to Deposit Cadmium on Metal

Electroplating is the most common means of cadmium coating accounting for over 90% of all applications. Methods called ion deposition, vacuum deposition and mechanical plating also are important.

2.2.1.1. Electroplating

An electrolyte solution of cadmium salts is the medium used to deposit cadmium on the metal article in question. [7] The most commonly used electrolyte solutions are the alkaline cyanide systems. Fluoroborates are also used, the outcome is not as bright, covering power and throwing power are comparatively low and operating parameters

are narrow compared to the alkaline cyanide system. Metal to be coated is cathode cadmium from the anode goes into solution and then deposited on the metal when a current is passed through the selected electrolyte. Depending on the size of the material to be coated either vat – plating by attaching the metal to racks or the use of a rotating barrel or vat – plating as the parts are placed in drum cages are the options. Former is used for coating large or delicate articles whereas the latter is preferred for clips, springs, washers, nuts bolts and similar small components.

2.2.1.2. Mechanical Plating

In this method mechanical energy is used to deposit metal coatings on small components and this is achieved by the impact of glass beads. It is applied in a rotating barrel. A mixture composed of the metal powder, water and proprietary chemicals along with glass beads used as the applicator is filled in this barrel and the components are added and these are all tumbled. Cadmium or else mixed-metal coatings of cadmium-zinc or cadmium-tin can be applied by this method. Method is suitable for coating of components small enough to be coated in a barrel such as fasteners and clips.

2.2.1.3. Vacuum and Ion Deposition

In this method cadmium is heated in a vacuum until vaporization. The result is a thin high-quality layer of cadmium that is formed by cadmium atoms that condense on the substrate. If argon atmospheres are to be used for ion deposition than sputter cleaning is applied to the substrate surface for cleaning purposes. This ion deposition results in improved coating adhesion, density and uniformity.

As the as coated surface is very delicate usual chromates that result in black, yellow, olive or clear finishes are applied.

Due to high toxic properties of cadmium it is not suitable for applications where the surface is intended to be in direct contact with food. Providing a very strong, superior

protection in brackish and aquatic applications cadmium coatings are commonly used in aerospace and harsh environments.

2.3. Hydrogen Embrittlement Phenomenon and Its Relation to Cadmium Coating Process

Hydrogen embrittlement can be defined as “a metal’s loss of ductility and reduction of load bearing capability” which is a result of hydrogen atoms or molecules being absorbed by the base metal. [8] Premature failure or cracking of the components before their service life is the result of hydrogen embrittlement.

Absorption of hydrogen atoms by carbon steel alloys can be observed even at room temperature. It is important to note that the studies suggest the source of the hydrogen that enters the steel body does not have a significant importance nor changes the mechanism of failure. Similarly, hydrogen absorbed may be present in both in the atomic form or in the molecular form. Diffusion here is time dependent, after sufficient time passes the hydrogen diffuses to the metal grain boundaries. Then this diffused hydrogen forms bubbles at the metal grain boundaries that results in pressure to be exerted on the metal grains. This pressure exerted on the grain boundaries by hydrogen bubbles formed can increase to levels certain levels resulting in reduction of ductility and strength of the metal. [9] – [12]

Below is a schematic representation of the explained above phenomena.

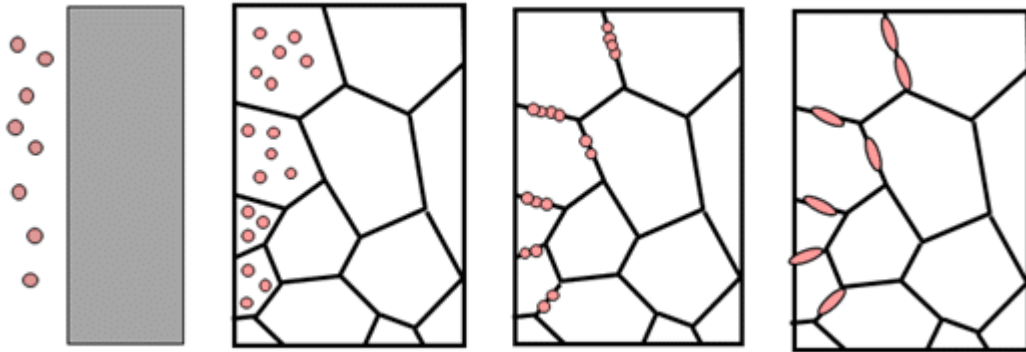


Figure 2.1. Hydrogen bubble migration to grain boundaries and formation of bubbles along these sites [13]

Hydrogen uptake is known to occur during various manufacturing and assembly operations or during actual service of the manufactured part or component. Whenever the metal comes into contact with atomic or molecular hydrogen uptake can take place.

Phrases hydrogen attack or hydrogen induced cracking are also used interchangeably with hydrogen embrittlement. Electrolytic tough pitch copper, aluminum alloys and titanium alloys are materials that are known to show most vulnerability to hydrogen along with high-strength steels. Both aqueous or gaseous mechanisms be involved in hydrogen embrittlement.

Below given is a schematic representation of both mechanisms:

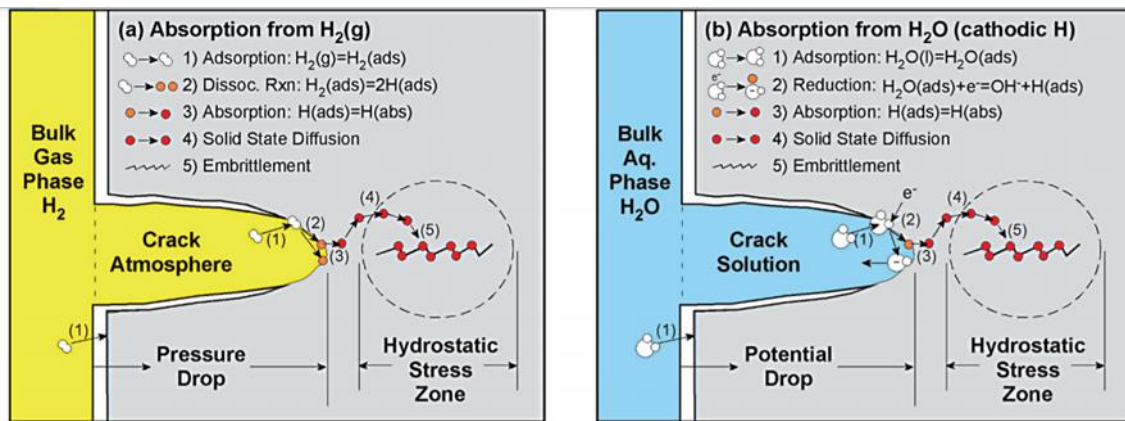


Figure 2.2. Hydrogen uptake from (a) Gaseous Environment and from (b) Aquatic Environment [14]

Acid pickling and electroplating are two processes which involve possibility of hydrogen absorption. Acid pickling baths have hydrogen in used solutions by nature. During electroplating process, at the surface of the metal being coated hydrogen production occurs. Acid pickling is a form of surface treatment commonly used to remove oxide scale and other contaminants from the surface of steel and this pre-treatment also prepares the surface of the substrate for the plating operation by increasing the surface area. Electroplating is commonly used to deposit several metals like zinc and chromium with galvanic corrosion protection properties on steel nuts, bolts, screws and other fasteners. Note that there are other metals used for electroplating to serve different purposes specific to various applications.

During service hydrogen absorption can also occur when the steel component in question is exposed to acids or if corrosion of the steel occurs. Pipelines usually show this susceptibility.

Intergranular cracking is the phenomena in a metal body where the cracks are formed on the grain boundaries and they grow along these boundaries. Similarly, hydrogen bubbles resulting in hydrogen embrittlement are known to settle at grain boundaries weakening the structure.

The exposure of a susceptible material to an environment that contains hydrogen in presence of tensile stress on the component are the three requirements to be present for failure due to hydrogen embrittlement.

High-strength steels that have tensile strength greater than approximately 1000 MPa are determined to be the most vulnerable the alloys when hydrogen embrittlement is considered.

Once the hydrogen is picked and settled at grain boundaries even a tensile residual stress within a component can cause fracture.

Reduction of hydrogen exposure is a good solution to prevent embrittlement whenever possible. Hydrogen relief baking after processes like electroplating that are known to lead to hydrogen absorption is a common precaution taken to avoid hydrogen embrittlement. It has become a standard industrial practice to bake parts between 190 to 220°C for at least 4 hours and usually 8 to 24 hours within the minimum time spent after electroplating. If applied in a timely manner during this baking operation absorbed hydrogen would diffuse out of metal. One thing to be considered is that this additional heat-treatment must not compromise any of the other desired mechanical properties of the coated metal.

Unfortunately, it is not always possible to avoid exposure to hydrogen during service. For those applications where there will certainly be hydrogen absorption lower strength steels are selected and residual and applies stress is minimized as a precaution to avoid embrittlement.

It was observed by Johnson as early as year 1875 that toughness along with breaking-strain of iron changes in extraordinary manner once the material in question is temporarily immersed in acid for no more than just a few minutes. One of the interesting results of this observation is that this is not a permanent change. In his words; “with the lapse of time, the metal slowly regains its original toughness and strength”. He further observed a phenomenon referred to as frothing where gas bubbles that are even visible under oil are liberated from surface of the embrittled steel

once the fracture surface is moistened. In his studies he also suggested that immersion of a stronger steel in acid will result in a greater loss in toughness compared to a soft one. Although he used several acids for this study, he observed that only the acids that would produce hydrogen on iron lead a deterioration of properties. Interestingly leaving the same steels used in the study in hydrogen gas did not lead to the same outcome. After this observation he designed an electrochemical aiming to separate out the effect of hydrogen from the effect of acid and proved that only the iron electrode where liberation of hydrogen occurred exhibited embrittlement. His research back in 1875 concluded that the source of embrittlement in steel was the hydrogen itself but not the acid and the hydrogen should be nascent rather than molecular and as diffusible hydrogen is the creator of embrittlement the phenomenon is reversible and frothing (bubbles) was the proof of this suggestion. Finally, he concluded that the as strength of the steel increases so does the susceptibility to hydrogen embrittlement. Following 50 years established further the role of nascent hydrogen. Relation of embrittlement to microstructure was another advancement in this topic. One of the studies carried out by Pfeil [15] showed that larger the grain size the more sensitive is the sample to hydrogen and sensitivity decreases where the structure has fine grains. Another conclusion drawn by Pfeil [15] was that although hydrogen was the reason that the cohesion across cubic cleavage planes decrease, slip was not affected and hydrogen created embrittlement in single crystals of iron. Although modern understanding challenges the details of Pfeil's [15] and other contemporary work especially on topics cohesion or slip approximately 38,000 papers that were published from that date on hydrogen embrittlement create no fundamental changes on the summarized above conclusions. One interesting phenomenon observed in diffusion measurements is that sometimes diffusible hydrogen is trapped at boundaries or other sites and these in certain cases are sufficient to strongly trap the hydrogen so no harm occurs in steel. Furthermore, controlling diffusible hydrogen is a necessity to produce hydrogen resistant steels. Introduction of benign traps in the steel or preventing the ingress of hydrogen are two means of achieving this.

Cadmium used to be the most widely used sacrificial coating in marine applications but due to its toxic properties this is no longer an option but the aeronautical applications still stand as no efficient replacement is in the market yet. Various studies are conducted to evaluate availability of replacement coatings along with determination the effect of hydrogen on different steels that are coated with various metals. We will now look deeper into a study on these effects. As can be seen below both cadmium and tin have hydrogen diffusion coefficients much smaller than ferrite. This property also acts as a barrier to hydrogen permeation.

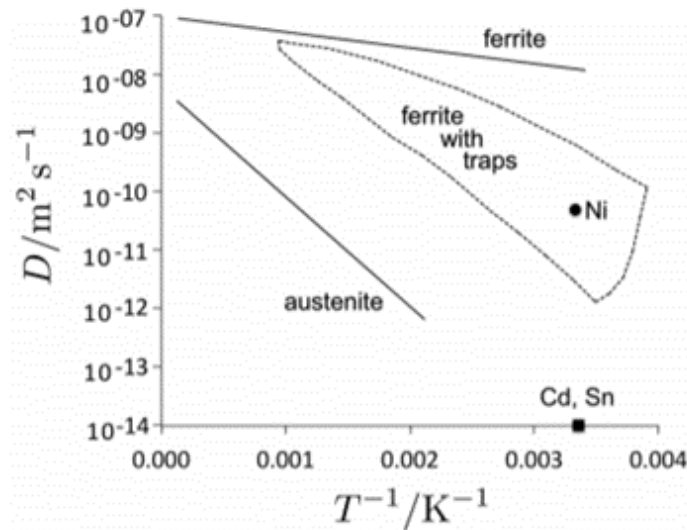


Figure 2.3. Diffusion coefficient of hydrogen in ferrite and diffusion coefficient of hydrogen in austenite. diffusion occurring in ferrite with strong traps is represented by the dashed region. hydrogen's diffusivity in nickel, cadmium and tin at ambient temperature is also represented [13]

As mentioned above hydrogen is introduced into base metal through coating processes and due to fact that nickel present will be deposited first to favorable sites forming a diffusion barrier to hydrogen as shown above penetration of hydrogen into steel is reduced significantly by alloying zinc with nickel. When nickel is plated on steel it will act as a diffusion barrier to hydrogen; at room temperature the diffusivity of

hydrogen in nickel is $5 \times 10^{-11} \text{ m}^2 \text{ s}^{-1}$. This effect is only viable if nickel coating is in a manner where hydrogen is not introduced into the steel. Below in Table 2.3 embrittlement indexes are given for AISI 4340 steel and 300M alloy that are coated with different metals being cadmium, zinc and a combination of zinc and nickel. As can be seen AISI 4340 is more susceptible to embrittlement compared to 300M on the other hand AISI 4340 shows greater improvement compared to 300M when zinc – nickel coating is applied rather than cadmium coating. This study was run by Figueroa and Robinson and they suggested this effect is resulting from the defects that are present in the zinc – nickel coating that leave some of the steel exposed, yet the reason why this behavior is exhibited by 300M steel is yet not clarified. One suggestion is that the relatively higher silicon present in 300M compared to AISI 4340 is responsible for this as due to this silicon presence surface quality is relatively poor at 300M. Moreover, absorbed hydrogen’s ability to reunite in its molecular form than create bubbles and escape before entrapment is also a factor along with diffusivity. As cadmium amount in the coating increases mentioned above recombination rate of hydrogen ingress is reduced.

Table 2.3. *Embrittlement index comparison of AISI 4340 and 300m after application of the given coating [13]*

<i>Alloy</i>	<i>Coating</i>	<i>Embrittlement Index</i>
AISI 4340, Quenched and Tempered	Cadmium	0.78
AISI 4340, Quenched and Tempered	Zinc	0.78
AISI 4340, Quenched and Tempered	Zn – 10 Ni wt%	0.037
300M, Quenched and Tempered	Cadmium	0.54
300M, Quenched and Tempered	Zn – 14 Ni wt%	0.46

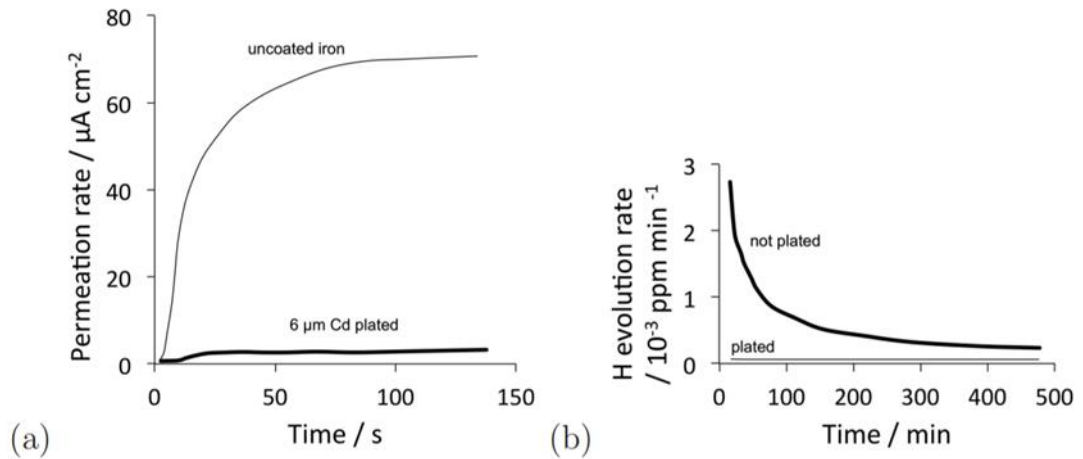


Figure 2.4. (a) Permeation rate of hydrogen to uncoated steel vs steel coated with 6 μm cadmium (b) comparison of hydrogen evolution rates under same conditions given in (a)

It is widely accepted that the damage to steel is created by diffusible hydrogen so to mitigate its effects methods that would render it immobile should be efficient. The experiments run by Darken and Smith shown that the absorption rate of hydrogen during charging is much faster than the hydrogen evolution rate from a charged specimen. Furthermore, a much higher saturation hydrogen content was observed at a cold-rolled steel sample compared to the one that is hot-rolled. They draw the conclusion that hydrogen can be localized at any kind of “departures or disturbances of, from the ideal lattice” at dislocations or at other and any form of non-ideal lattice are expected to act as an obstacle to the diffusion of hydrogen. It would not be wrong to state that there exists a general and physically justifiable consensus about the reduction in the susceptibility of the steel to hydrogen embrittlement under the presence of strong traps as there is an increase in the saturation hydrogen content due to the presence of traps but this trapped hydrogen is innocuous. Although it is stated that “on X80 pipeline steel that the large density of traps on the steel increases its susceptibility to hydrogen-induced cracking” in a recent paper, this suggestion does not seem to be viable as it is only based on the fact that more hydrogen is absorbed by the steel in presence of these traps.

The phenomena of delayed fracture where spontaneous brittle failure after a period of time in service occurs at a high strength steel subjected to a stress that is small relative to its original fracture strength measured right after manufacturing process is also worth mentioning. Hydrogen is suspected to be responsible of this type of failure under static load. An example to decrease in fracture strength of hydrogen charged samples where charging is achieved by electrolytical means can be seen from the graphical representation of a certain set of data is given below. There is data suggesting that if a stress that is greater than 600 MPa is applied to any component in service fracture would occur after a short period time.

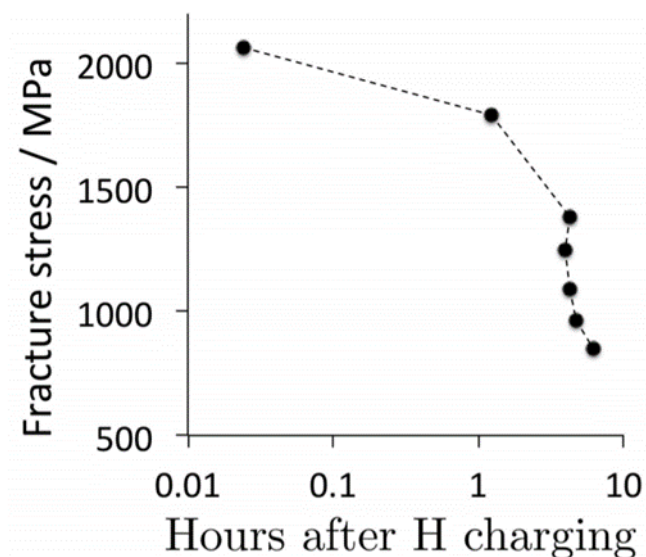


Figure 2.5. The change in fracture stresses of a high strength (1516 MPa) steel alloyed with nickel, chromium, molybdenum that is electrically charged with hydrogen over time after hydrogen charging

2.3.1. Industrial Trends in Testing Methods for Hydrogen Content Determination: 200 Hour Test vs 8 Hour Test

As suggested in the aerospace material specification AMS-QQ-P-416 published by SAE under the name “Plating, Cadmium (Electrodeposited) Standard Test Procedure”

for determining the hydrogen content of the coated sample is to subject it to 75% of either the notched ultimate tensile strength or yield strength of the base material for 200 hours followed by an examination for conformance. The procedure for 200-hour test is defined in “ASTM F519 – Standard Test Method for Mechanical Hydrogen Embrittlement Evaluation of Plating/Coating Processes and Service Environments”. Although the 200-hour test is still used by the industry it is a very time-consuming method. In most cases the coated parts are dispatched before the results are obtained from the 200-hour test that takes 9 to 10 days and any fail would require recall of all dispatched parts. As an alternative for industrial applications an accelerated version was proposed by Drehler on a Special Technical Publication of ASTM [16]

A step load test is chosen to discriminate between the overload failure and embrittlement because hydrogen embrittlement is enhanced by slow strain rates. The underlying mechanism may be accumulation of hydrogen near dislocation sites of micro voids but the precise mechanism is still unknown.

The accelerated test will be referred as 8 – hour test from now on. 8 – hour test shall be run within the first 48 hours to give healthy results.

2.4. Determination of Fatigue Behavior Using S – N Curves and the Effect of Hydrogen

Cracks; growth rates of cracks, stress intensity factors at cracks, stress fields around cracks, failures due to cracks, are all investigated under the name fracture mechanics. [17]

Fracture mechanics date back to 1898 where researchers tried to find analytical solutions for stresses at holes. Then in 1913 they carried on investigations now ellipses being the main subject of interest. In 1920 Griffith ran energy-based crack analysis and this is considered as the official start of research on fracture mechanics.

The Second World War has significant importance on research on fracture mechanics. After cases of sudden failure of ships and aircraft during the war, cracks that are

considered small and insignificant became a major area of interest as they were found responsible of these catastrophic failures of these majestic structures.

Fatigue life basically is the duration a metal part can withstand different modes of loading. It is a complicated process to predict the fatigue life of a metal part as it is observed that minor changes in loading conditions and stress concentrations along with several other factors have great effects on the fatigue life. Manufacturing procedures such as cold forming, welding, brazing, and plating also affect the resistance of a metal structural member to fatigue and so does surface conditions such as surface roughness and residual stresses. It should also be noted that fatigue tests performed on small specimens are good for determination of baseline properties of the material in question under cyclic loading and create relative resilience ratings but not sufficient if the aim is to precisely establish the fatigue life of a part. It is still a viable approach to combine these baseline properties determined with the load history of the part and then run a design analysis to predict the service life of a certain component.

If this kind of a design analysis is to be made the type of applied loading namely the load being uniaxial, bending, or torsional; the loading pattern such as the load either being applied in a periodic manner or at a constant or variable amplitude or application of random load; magnitude of peak stresses, should be considered along with overall size of the part, method of fabrication, surface roughness values, if fretting or corroded surfaces are present, operating temperature and operating environment, and occurrence of service-induced imperfections should also be taken into consideration and so does the material properties and loads. Traditionally approach to expressing fatigue life has been the use of total number of stress cycles required for a fatigue crack to initiate and grow large enough to separate the sample into two which is regarded as catastrophic failure.

After the fatigue tests are finished the resulting data is tabulated by plotting the maximum stress or stress amplitude versus the number of cycles to fracture that is designated by “N”. The number of cycles is represented using a logarithmic scale.

Either a linear or a logarithmic scale can be used to represent stress. This graphical representation of the curve constructed by the collected data points is called an S-N curve or a Wohler diagram. If we look at an S-N curves that are plotted using a linear stress scale versus logarithmic scale for life that belongs to carbon and low-alloy steels we can see that the resulting curve would be composed of two portions; fairly straight slanting portion with a negative slope at low cycles, which changes into a straight, horizontal line at higher cycles with a sharp transition. Variability of material along with many other reasons result in the scatter of fatigue lives over a very wide range.

When laboratory tests are run to determine fatigue behavior for a certain material testing is done either with axial loading, or in bending, and the applied stresses are only tensile and compressive. Usually the cyclic stress loading mode is either tension between a maximum and a minimum, or between a maximum tensile stress and a maximum compressive stress. The stress ratio is the algebraic ratio of two specified stress values in a stress cycle. There are two commonly used stress ratios referred to as A for alternating stress amplitude to the mean stress and R to refer to the minimum stress to the maximum stress. If the stresses are applied in a fully reversed condition, the stress ratio becomes $R = -1$; whereas, R becomes a negative number which is less than 1 the stresses are partially reversed. R which is the designation used for the stress ratio becomes zero if the stress is cycled between a maximum stress and no load. R becomes a positive number less than 1 if the stress is cycled between two tensile stresses. A stress ratio $R = 1$ means there are no variation in stress, so the test becomes a sustained-load creep test and not a fatigue test.

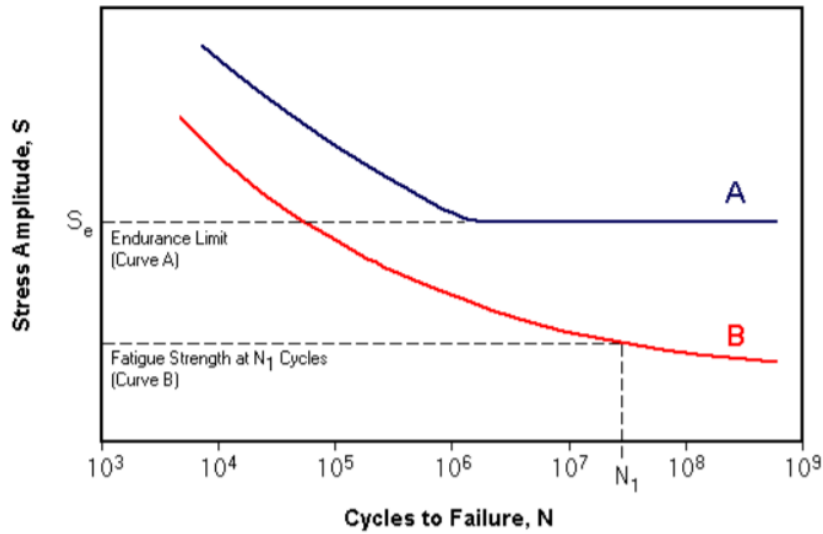


Figure 2.6. Sample S – N curves of two different materials, behavior of material A shows an endurance limit whereas material B does not exhibit an endurance limit [18]

For certain materials there is a certain stress level below which the material does not fail regardless of the number of cycles so cyclic load of such can be applied infinitely this stress amplitude is called fatigue limit or endurance limit. A structure manufactured from a material exhibiting endurance limit is said to have an infinite life if the applied stress level is below this determined limit. At loads below the endurance limit of the material in question, the structure composed of this material is said to have an infinite life. Steel and titanium would exhibit such behavior under favorable environmental conditions.

When plotted on a log-log scale, the straight-line portion of an S – N curve can be defined using a power law equation which is given as follows: [17]

$$N_1 = N_2 \left(\frac{S_1}{S_2} \right)^{\frac{1}{b}} \quad \text{Eqn.1}$$

In the given above equation the slope of the line is designated by “b”. It is sometimes called the Basquin slope, Basquin slope is given by the equation below: [17]

$$b = \frac{-(\log S_1 - \log S_2)}{\log N_2 - \log N_1} \quad \text{Eqn. 2}$$

The power law equation is used to calculate the cycles to failure for a known stress amplitude when the Basquin slope and any coordinate pair (N, S) on the S-N curve are known.

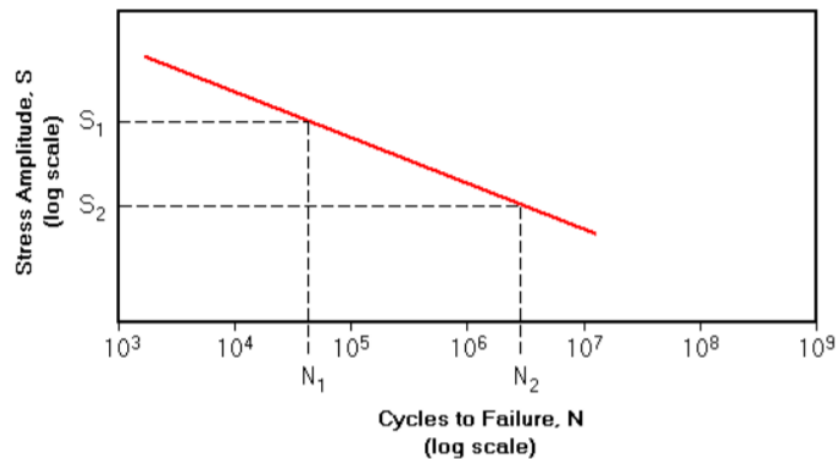


Figure 2.7. Graphical representation of the Basquin Slope

There are numerous studies [19] – [26] on fatigue life determination and effect of certain factors that change the fatigue behavior of different materials. [27] – [33] Some of these studies are mentioned in the following text.

Ronevich [34] studied the fatigue growth rate in X65 steels. It was found that fatigue growth rate was significantly higher in hydrogen gas. With regard to the pearlite orientation, the fatigue rate was lower in perpendicular bands than compare to the parallel axis. Therefore, it was concluded that hydrogen transport in the microstructure was dominant factor in determining the fatigue properties.

Colombo [35] studied the fatigue behavior of hydrogen charged Cr-Mo steels. It was reported that the sensitivity of the alloy was high to hydrogen embrittlement. The growth rate was high in the initial stage followed by a plateau with constant value and a rapid fracture in the final stage. The toughness was found to decrease 4 times in the

presence of hydrogen. In the absence of hydrogen, the second stage was found to follow a partial intergranular crack.

Yamabe [36] looked into the fatigue crack growth of low carbon steel in hydrogen environment. The alloy was subjected to several different cold work ratios. It was reported that as the cold deformation was increased, hydrogen diffusivity was decreased. Hydrogen assisted fatigue crack growth rate was increased due to the localized increased plastic strain around the crack tips.

Ogawa [37] studied the hydrogen induced crack growth in fatigue tests. It was found that fatigue life in air was equivalent to 0.7 MPa hydrogen gas. Thus, a ductile fracture was observed. As hydrogen gas was increased to 115 MPa, fatigue life was significantly reduced. The fatigue had exhibited no shear-lip but a completely flat brittle surface.

A study on the influence of hydrogen pressure on fatigue properties of X80 steel suggested that the low cycle fatigue life of the samples was decreased significantly in low pressure hydrogen but was increased with increased hydrogen pressure. Another finding of the same study is that when hydrogen gas was below 0.6 MPa, there was no noticeable change reported in the fatigue properties and crack initiation was increased with increased hydrogen partial pressure.

Ogawa [38] in another study looked into the metastable austenitic steels fatigue properties. The effect of external and internal hydrogen was compared. External hydrogen appeared to have more dominant effect on the fatigue crack growth rate. This was related with the hydrogen penetration efficiency.

Rustagi [39] modelled the hydrogen assisted fatigue crack growth in pipeline steels. He concluded that the fatigue crack growth is a function of hydrogen pressure which is mainly determined by the transportation of hydrogen to the crack tips. Thus, microstructure has intricate function.

Richardson [40] run thermal desorption analysis of hydrogen on data collected by rolling contact fatigue tests of non-hydrogen charged 100Cr6 steel.

Although there are no established rules explaining the exact mechanism of hydrogen embrittlement Gangloff [41] suggested three mechanisms that may be active being Hydrogen Enhanced Decohesion (HEDE) where transgranular fracture occurs due to hydrogen reducing atomic cohesion and slip is hindered; Hydrogen Enhanced Localized Plasticity (HELP) where hydrogen stimulates dislocation processes that localize plastic deformation sufficient to result in subcritical crack growth with brittle characteristics on the macroscopic scale and Adsorption Induced Dislocation Emission (AIDE) where intergranular cracking occurs due to hydrogen accumulation at grain boundaries.

CHAPTER 3

EXPERIMENTAL PROCEDURE

3.1. Material Used for the Experiments

A modified 4340 steel that was produced for a specific defense application by an entity not referred in this work due to the fact that the aim of this modification, production stage, heat treatment and final application being classified is used for all experiments. The steel referred to as modified 4340 was manufactured in an electric arc furnace, electroslag refining and vacuum degassing were applied than the molten metal was cast into 5 tones ingots that were forged into its final dimensions. The standard composition of AISI 4340 is given in Table 3.1

Table 3.1. *Standard chemical composition of AISI 4340 steel*

C	Mn	P	S
0.38 – 0.40	0.60 – 0.80	max. 0.035	max. 0.040
Si	Ni	Cr	Mo
0.15 – 0.35	0.65 – 2.00	0.70 – 0.90	0.20 – 0.30

The spectral analysis of Modified 4340 used in the experiments is given in Table 3.2. The sample cut from the billet's chemical composition was determined using optical emission spectrometer, WAS brand, model Foundry Master.

Table 3.2. Spectral analysis of the billet used to extract test samples used in this study

	<i>Fe</i>	<i>C</i>	<i>Si</i>	<i>Mn</i>	<i>P</i>	<i>S</i>
1	94.4	0.401	0.251	0.250	0.0159	0.0135
2	94.4	0.404	0.256	0.252	0.0133	0.0133
MEAN	94.4	0.403	0.253	0.251	0.0146	0.0134

	<i>Cr</i>	<i>Mo</i>	<i>Ni</i>	<i>Al</i>	<i>Co</i>	<i>Cu</i>
1	1.144	0.455	2.256	0.004	0.010	0.183
2	1.156	0.460	2.268	0.003	0.010	0.185
MEAN	1.150	0.458	2.262	0.004	0.010	0.184

	<i>Nb</i>	<i>Ti</i>	<i>V</i>	<i>W</i>	<i>Pb</i>	<i>Sn</i>
1	0.0191	<0.002	0.073	0.010	0.0375	0.0098
2	0.0174	<0.002	0.074	0.012	0.0394	0.0114
MEAN	0.0183	<0.002	0.074	0.011	0.0385	0.0106

	<i>B</i>	<i>Zr</i>	<i>As</i>	<i>Bi</i>	<i>Sb</i>
1	0.0027	0.0106	0.0224	0.002	0.0444
2	0.0030	0.0107	0.0202	0.003	0.0486
MEAN	0.0029	0.0107	0.0107	0.002	0.0465

3.2. Heat Treatment of the Base Metal

The modified 4340 steel ingot that was used in these experiments undergo the heat treatment cycles given below. The heat treatment operation was carried out by the source manufacturer of the material.

The heat treatment cycles were applied in an electric heated furnace with thermal stability of $\pm 5^{\circ}\text{C}$. The material was degreased and cleaned from any chemicals at the surface before the heat treatment application.

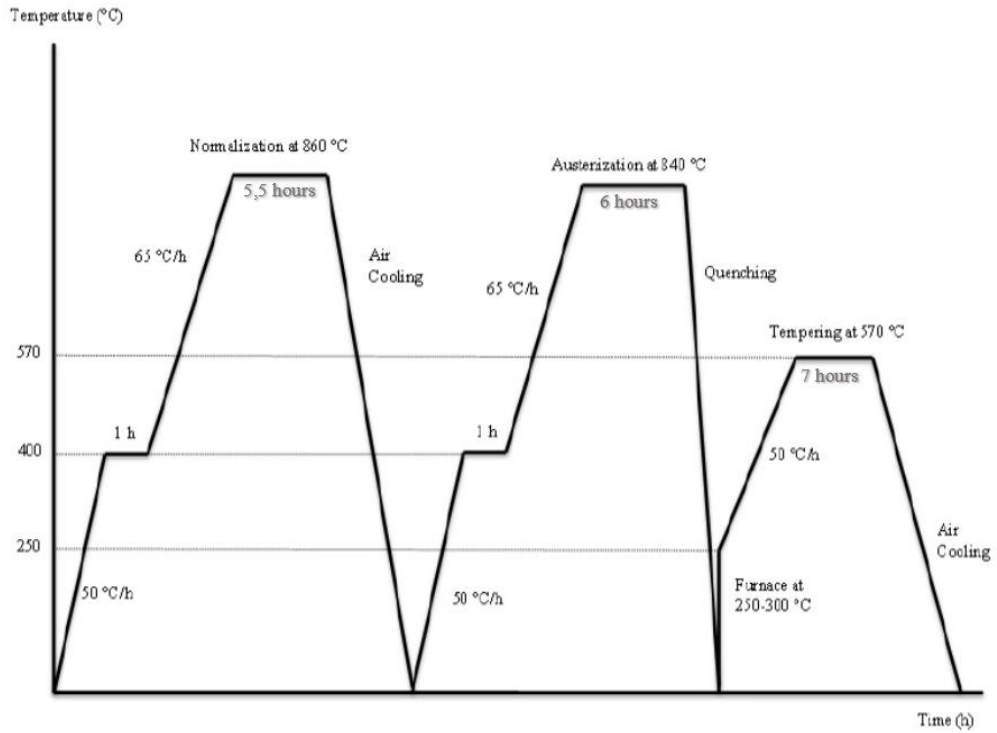


Figure 3.1. Heat treatment cycles that the modified 4340 steel used in experiments undergo (process parameters are supplied by the source manufacturer of the material)

The austenitized material was placed at the water quenching apparatus within 2 minutes of after removal from heat treatment furnace. The water quenching system seen below that has a rotation speed of 20 – 30 rpm. The water pressure was 2.8 ± 0.2 bars.



Figure 3.2. Setup used by the entity that manufactured the modified 4340 steel for the water quenching operation

3.3. Directions of the Samples Used in the Experiments

All the samples used in the experiments are cut from a cylindrical billet with 176 mm diameter and 240 mm of length.

Tensile specimen and rotating beam fatigue (hour glass) specimens are taken from z direction, hardness test and spectrometer measurements are carried on z plane, metallographic samples are taken from x, y and z planes.

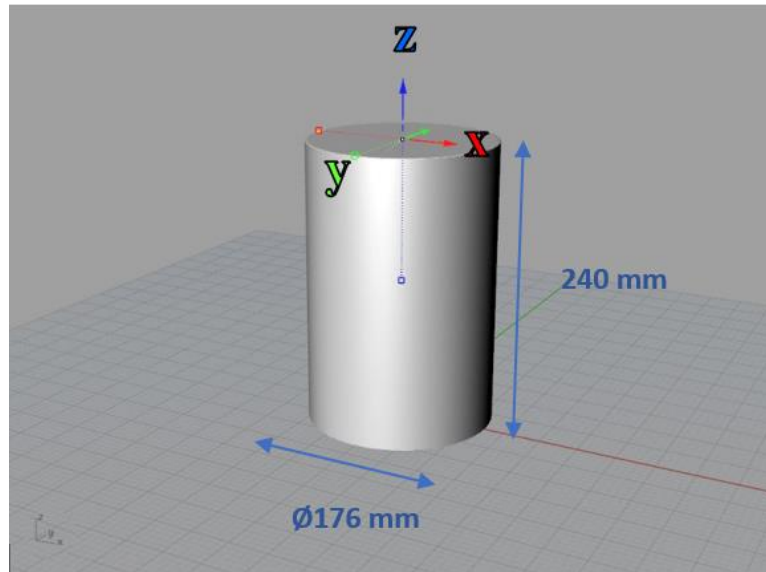


Figure 3.3. Representation of the modified 4340 billet and sample directions

3.4. Characterization of the Modified 4340 Steel Used in this Study

Spectral analysis, hardness tests, tensile tests and metallographic examination of the steel is done in order to determine its chemical composition and mechanical properties.

3.4.1. Metallography

Samples from all three directions were subjected to metallographically examined after surface preparation by grinding, polishing (Al_2O_3) and etching with 3% Nital solution. The microstructure was characterized by SEM.

3.4.2. Hardness Testing

Hardness values were measured on x-y plane by EMCO hardness indenter machine. Indenter ball diameter is 2.5 mm and the force applied is 187.5 kgF. Data is represented in Brinell hardness scale (HB).

3.4.3. Tensile Testing

A tensile specimen extracted along z direction of the billet was pulled to fracture to determine the tensile properties of the modified 4340 steel at the INSTRON universal testing machine

3.5. Coating Process

Steel was coated with cadmium as a part of this study and following tests were applied to these coated specimens of given size and shape.

All the specimens referred to as coated were coated with cadmium and then passivated in a chromium bath at the military facility 5th Main Maintenance Centre.

Given below is the flowchart of the cadmium coating process applied in 5th Main Maintenance Centre. The samples that were used in this study were coated as a part of this study under these conditions according to the process flow shown in Figure 3.4.

Degreasing	Pickling	Cyanide dip	Cd Coating	Cromating
<ul style="list-style-type: none"> • Solvon TMs • @ 70 – 75 °C 	<ul style="list-style-type: none"> • Hydrochloric Acid (40%) • Rodine 50 – 60 (60 %) • Normal procedure - dip for max 1 min 	<ul style="list-style-type: none"> • Sodium Cyanide • 15 – 45 g /l • @ RT • Max 1 min • Aim is to conserve the plating medium and protect it from the acid 	<ul style="list-style-type: none"> • Cadmium Oxide (27 g/l) • Sodium Cyanide (105 g/l) • Sodyum Hydroxide 7.5 g/l) • Sodium Carbonate 7.5 g/l) • @ 15 – 27 °C • 10 Amperes • 1.5 Volts 	<ul style="list-style-type: none"> • Potassium Dichromate (8 – 10 g /l) • Hydrochloric Acid (2-3 ml/l) • @ RT • To passivate the surface

Figure 3.4. Schematic representation of cadmium coating process. Each step is followed by a washing (cold rinse) operation to prevent contamination of the baths and inhibit complications like over etching.

Etching and plating parameters used in this study are given below in Table 3.3.

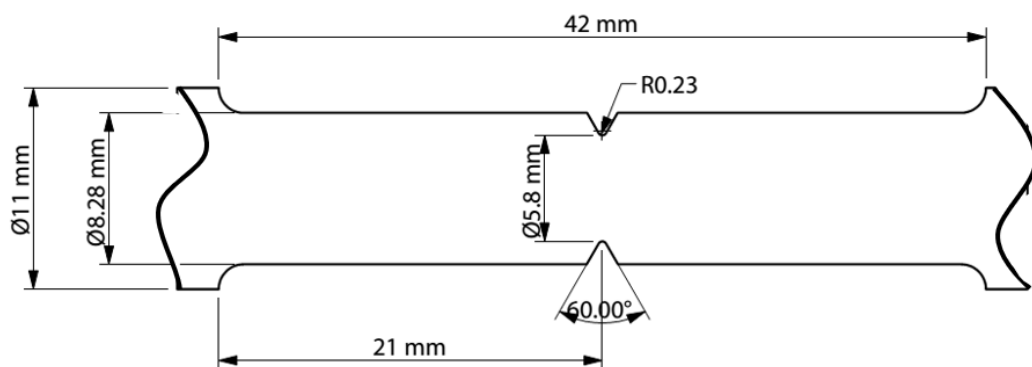
Table 3.3. Etching and coating parameters

<i>SAMPLE</i>	<i>ETCHING</i>	<i>COATING</i>
1	2 min	4 min
2	2 min	8 min
3	4 min	4 min
4	4 min	8 min

3.6. 8-Hour Test

The samples were machined to the dimension given in Figure 3.5. They were subjected to 8-hour test conducted at the INSTRON universal testing machine.

In 8-hour, test, notched samples of shape and dimensions given in Figure 3.5 and tabulated in Table 3.5 were step loaded with loads given below in Table 3.4, starting from 50% of load at fracture and each step lasts for an hour. The coated notched samples and the sections where the coating thickness was measured can be seen on Figure 3.6.



Scale 4:1

Figure 3.5. Dimensions of the gauge section of the notched specimen used in the 8-hour tests

Table 3.4. *Loads used for the 8-hour test*

<i>% of the Baseline Fracture Load</i>	<i>Nominal Value of the Load (N)</i>
50	32260
65	41938
75	48390
85	54842
90	58068
95	61295
Pull to fracture	No fracture at any load less than 2% of the baseline fracture load
100	64521

Samples are held at each step for one hour and then the test is continued by the load increasing incrementally as shown in Table 3.4 at the end of each session until the fracture occurred.

If the sample fails to finish the test, it is suggested by Drehler that there shall be a certain extent of hydrogen within the sample.

Table 3.5. *Dimensions of the notched tensile specimen in conformity with ASTM E8*

<i>Location</i>	<i>Dimensions</i>
End \varnothing	11 mm
Gauge \varnothing	8.28 mm
Notch \varnothing	5.8 mm
Notch Angle	60°
Notch Radius	0.228 mm
Gauge Length	32 mm



Figure 3.6. Two sets of identical cadmium coated, notched tensile specimens and sections cut to measure thickness molded into Bakelite. Etching and coating parameters are given in Table 3.3

3.7. Rotating Beam Fatigue Test

Two batches of coated samples were prepared for rotating beam fatigue test. Each batch consisted of 5 samples that are etched and coated using conditions given in Table 3.6. A set of 5 uncoated samples were also tested under the same test loads to be able to compare the fatigue behavior of the coated samples with the as machined material.

Table 3.6. Conditions selected for rotating beam fatigue testing

Sample Set	Etching	Coating
1	2 min	8 min
2	4 min	4 min
3	4 min	8 min

The test equipment used for rotating bending test is given in Figure 3.7. The stress ratio selected was $R = -1$ which indicates a fully reversed stress loading. Frequency used during all the tests was 50 Hz.

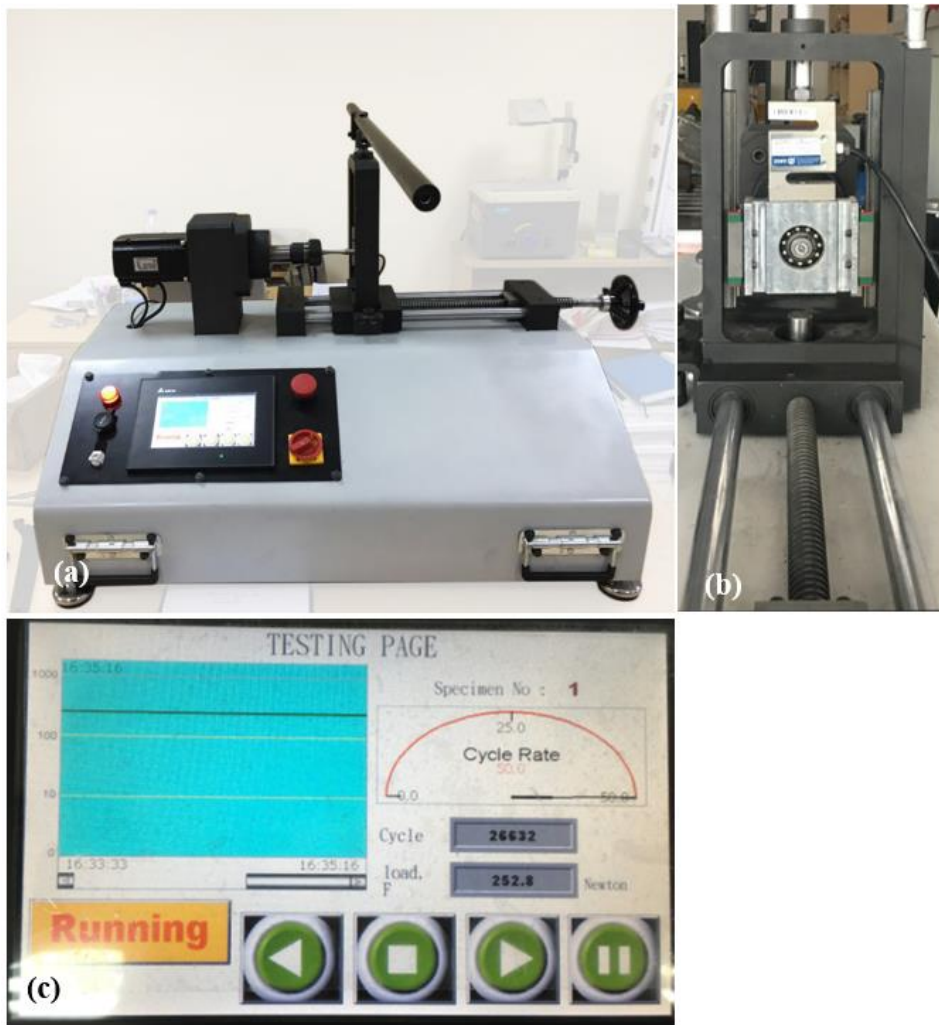


Figure 3.7. Rotating beam testing machine (a) general appearance (b) closer look to the rotating end and the load cell above the fixture (c) data screen

Rotating beam fatigue samples were machined to the standard dimension in conformity with ISO 1143:2010 as given in Figure 3.8

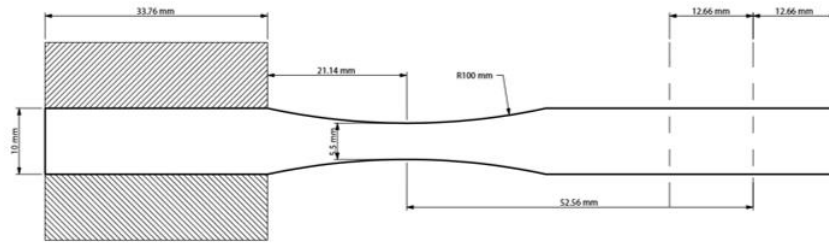


Figure 3.8. Rotating beam fatigue specimen, technical drawing and the actual sample

Samples were divided into two groups: unloaded and preloaded for the rotating beam test. Instron 5582 tensile test machine was used to load samples (referred to as preloading operation within this text) under the following conditions: 1 mm/min, 75% of the baseline fracture load which corresponds to 48390 N for 1 hour. The reason for the preloading was to keep the samples under tensile tension in an aim for forcing the hydrogen to migrate to the grain boundaries

CHAPTER 4

RESULTS AND DISCUSSION

4.1. Microstructural Analysis

After the samples were prepared by grinding, polishing and etching, they were subjected to SEM for microstructural analysis. The results are given in Figure 4.1. As can be seen for all the samples, tempered martensite constructs the structure. Some inclusions were observed in the microstructure in the size of 10 microns which were occasionally round and spherical as well as elongated shapes.

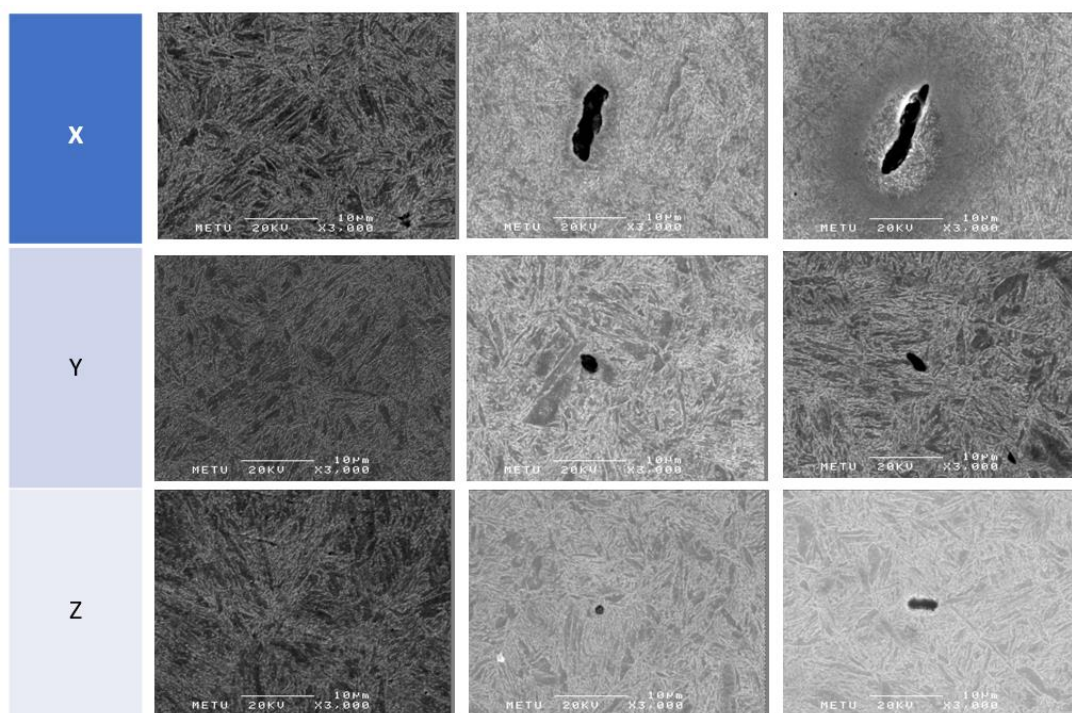


Figure 4.1. SEM images of the microstructure taken from samples cut from x, y and z directions under 3,000x magnification. First column is the general appearance, some inclusions can be seen on 2nd and 3rd columns.

4.2. Hardness Measurements

The billet was sectioned from the center and hardness was measured from one edge towards the other edge along x-y direction, measurements were taken with approximately 15 mm distance from each other as seen in Figure 4.2. The results are given in Table 4.1 The mean value of all ten measurements is 443 ± 11 HB

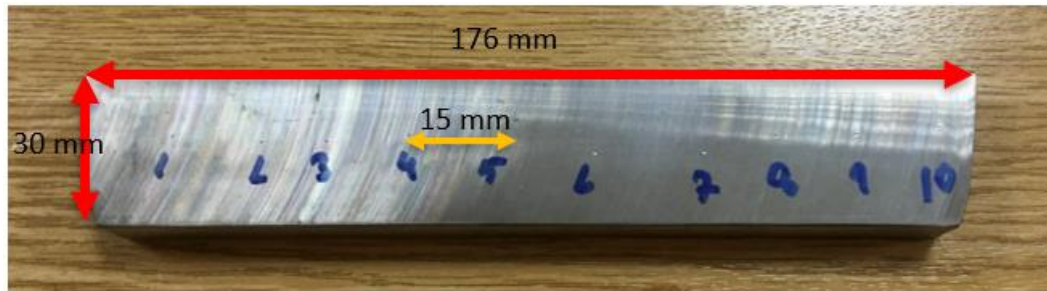


Figure 4.2. Hardness measurement points and the actual section used for these measurements

Table 4.1. Brinell Hardness measurement results related to points specified at Figure 4.2

Point	1	2	3	4	5	6	7	8	9	10
HB	447	430	440	464	454	442	448	438	439	429

As seen from Table 4.1, the hardness change along the diameter of the ingot was so consistent and the scatter of the results were very low. There is no indication of a decrease from the circumference to the core which indicates the through hardening of the billet was achieved via the applied heat treatment process.

4.3. Tensile Properties

A standard tensile test specimen was used to determine the tensile properties of the modified 4340 steel and the related data is tabulated in Table 4.2.

Table 4.2. Tensile test results

<i>Yield Strength (0.2% offset) (MPa)</i>	<i>Ultimate Tensile Strength (MPa)</i>	<i>Elongation (%)</i>
1244	1359	14

4.4. Properties of the Coating

4.4.1. Coating Thickness

After the coating process, the resultant thicknesses were measured using Scanning Electron Microscope (SEM). The related images are given in Figure 4.3. The coating thickness values were summarized in Table 4.3

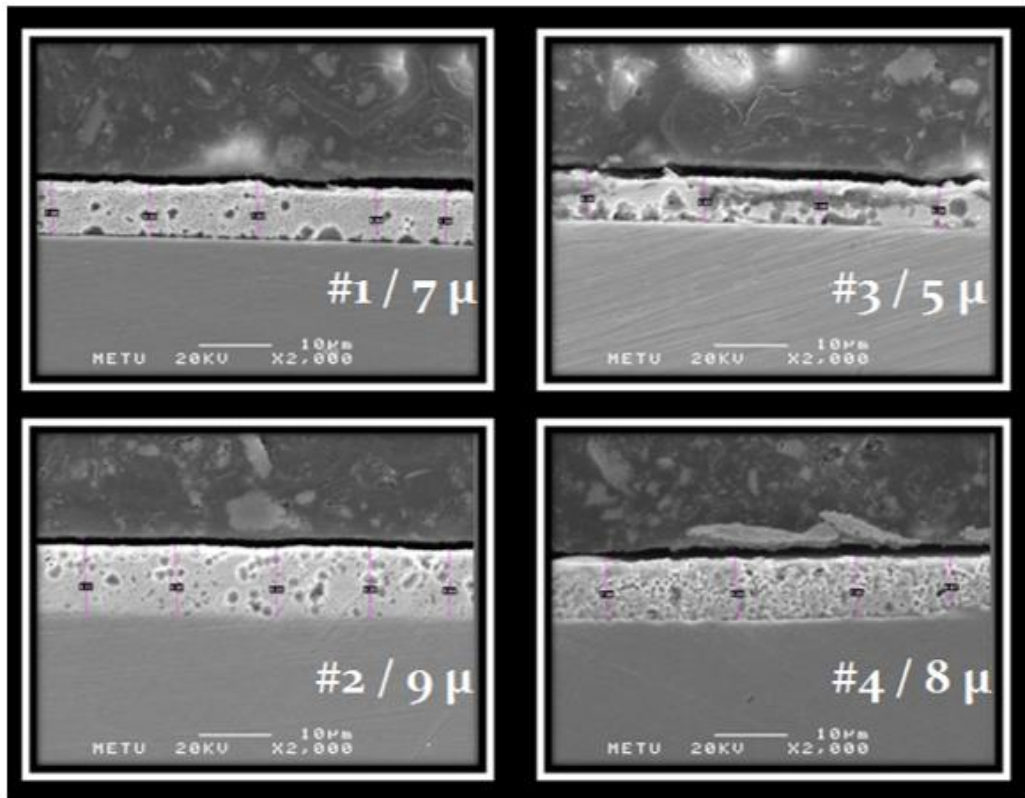


Figure 4.3. The coating thicknesses measured under SEM

Etching and plating parameters and the resulting coating thicknesses of the conditions 1 to 4 are given below in Table 4.3.

Table 4.3. *Coating thicknesses that resulted from given etching and plating parameters*

<i>Sample</i>	<i>Etching</i>	<i>Coating</i>	<i>Thickness</i>
1	2 min	4 min	7 μm
2	2 min	8 min	9 μm
3	4min	4 min	5 μm
4	4 min	8 min	8 μm

As can be seen from Table 4.3, as coating duration was increased from 4 to 8 minutes, there is no significant increase in the coating thickness. There is approximately 2 μm change for both conditions.

The obtained thicknesses were in correlation with the applied procedures but they were comparatively thin as 5th Main Maintenance Centre's regular practice and process parameters. At this point it should not be forgotten that the deposition rate is not a linear function of time.

4.4.2. SEM Images of the Coated Layer

Below the SEM images of the cadmium coated layer can be seen from the surface (in chromate passivated condition) and from cross section. The deposited layer of chromium is dendritic and columnar like in appearance and contains pores.

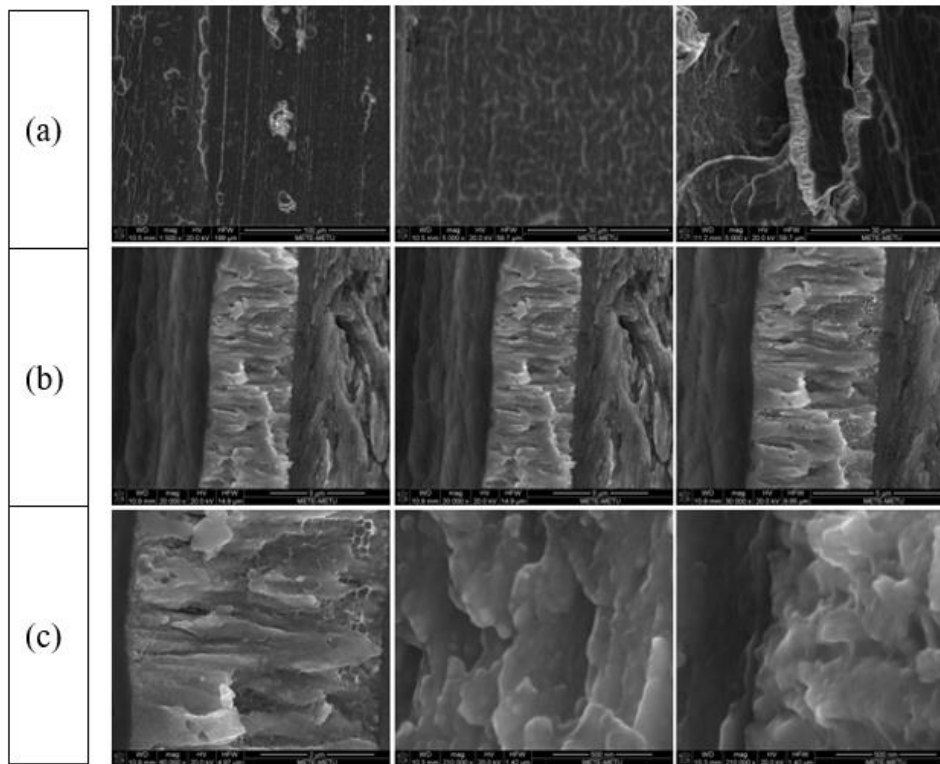


Figure 4.4. SEM images of the electrodeposited cadmium layer. (a) Top row is the appearance of the surface of the coating, (b) second row the cross section can be seen and (c) a closer view to the coating inner structure is given on the third row

4.4.3. EDS Analysis of the Coated Layer

The EDS analysis of the coating suggests that the inner layers of the coating is 100% cadmium as expected and the outer surface with the passivated finish is composed of roughly 85% cadmium and 12% chromium. The EDS data is collected from the middle of the cross section of the coating and a section closer to the surface respectively.

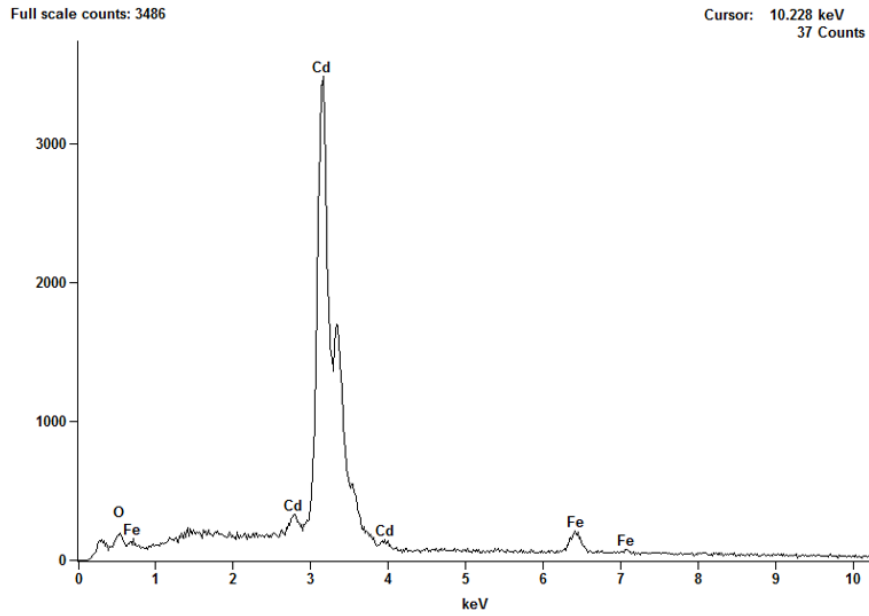


Figure 4.5. EDS spectra of the coating layer from the middle of the coating thickness

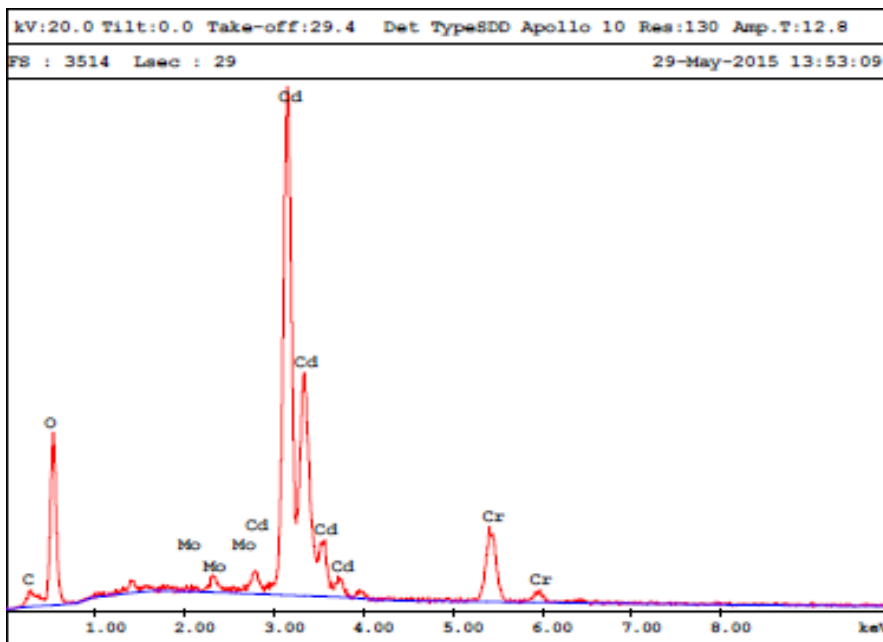


Figure 4.6. EDS spectra of the coating close to the passivated surface

Table 4.4. Distribution of chromium and cadmium close to the surface

Element	Weight %	Atom %
Cadmium	85.42	74.24
Chromium	12.68	23.82

4.5. 8-Hour Test Results

Given below at Figure 4.7 and Figure 4.8 are the graphics representing the behavior of uncoated and notched, round tensile specimen during 8-hour step load test and the related mechanical properties are tabulated in Table 4.5. The uncoated sample succeeded the test not breaking till pull to fracture. On the other hand, as can be seen from the data given in Table 4.6. all coated samples failed during 3rd or the 4th cycle under tabulated loads, which is regarded as an indication of possible hydrogen presence in the structure.

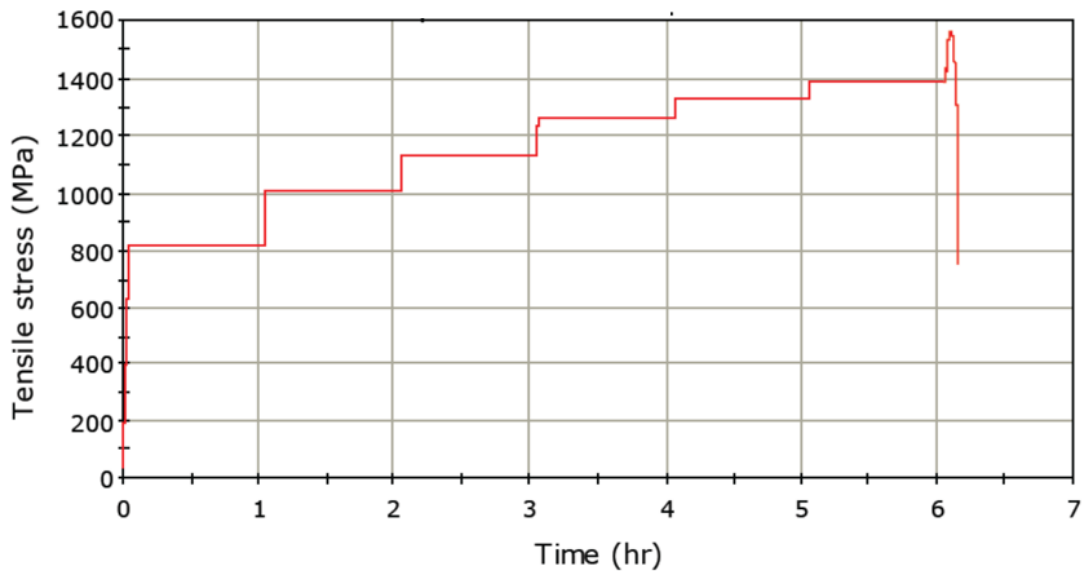


Figure 4.7. Time vs Tensile Stress graph of uncoated and notched, round tensile specimen made of modified 4340 steel subjected to 8-hour test. Sample finished the test and met the criteria so it is accepted that no hydrogen is present in the structure

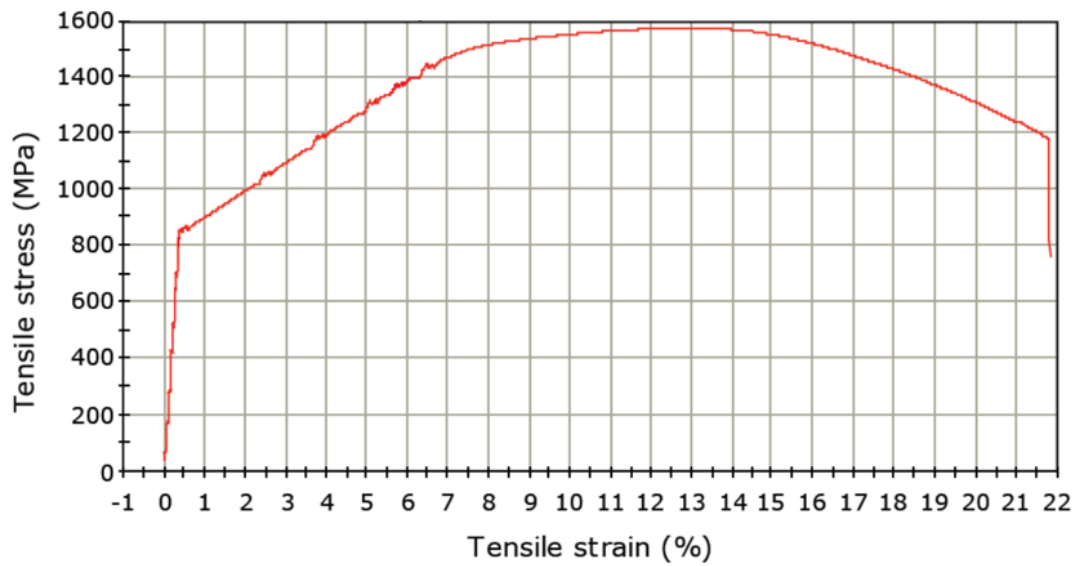


Figure 4.8. Stress vs Strain curve obtained from the 8-hour test of uncoated and notched, round tensile specimen made of modified 4340 steel

Table 4.5. Mechanical data obtained from the 8-hour test of uncoated and notched round specimen

<i>Axial Strain at Break (%)</i>	<i>Load at Break (N)</i>	<i>Tensile Stress at Break (MPa)</i>	<i>Maximum Tensile Stress (MPa)</i>
0.28865	63236	1197	1593

<i>Load at Max. Tensile Stress (N)</i>	<i>Axial Strain at Yield (2% offset) (%)</i>	<i>Tensile Stress at Yield (2% offset) (MPa)</i>
70025	0.28865	883

The fracture surface of the uncoated sample subjected to 8-hour test is given on Figure 4.9 The appearance is suggesting typical ductile fracture.

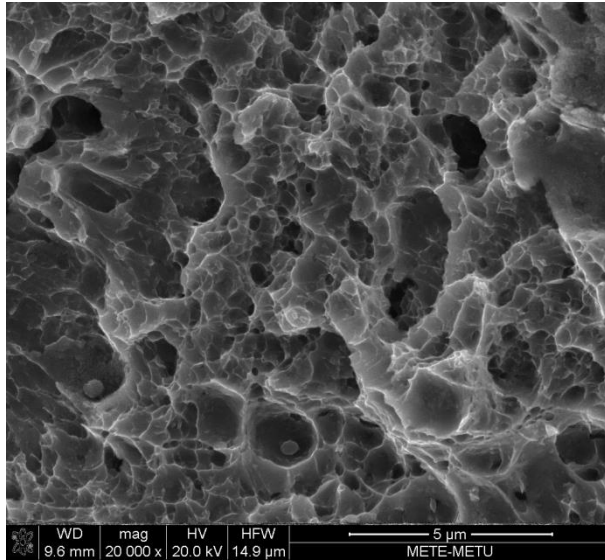


Figure 4.9. SEM image of the fracture surface of uncoated specimen subjected to 8-hour test taken from the core (magnification 20,000x)

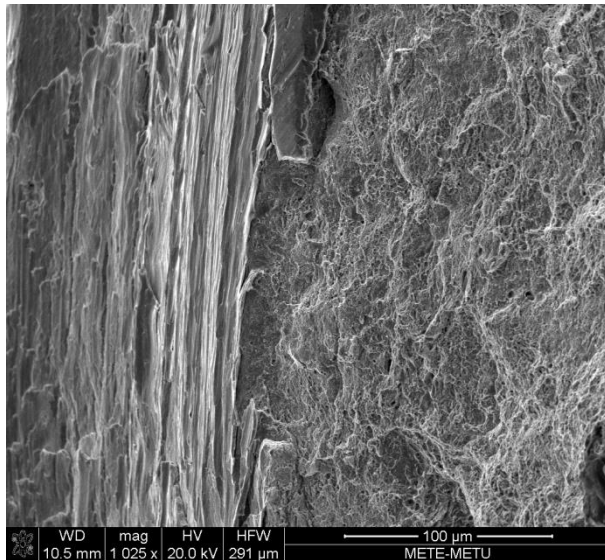


Figure 4.10. SEM image of the fracture surface of uncoated specimen subjected to 8-hour test taken from the modified 4340 steel and cadmium coating interface (magnification 1,025x)

Below in Table 4.6 the summary of the results obtained from the four coated specimens is represented. As stated earlier all coated samples failed during the 3rd or

4th cycles, prior to finishing of the test procedure. Related graphics and related mechanical properties are also given below.

Table 4.6. Summary of results of 8-hour load test composed of cycles to break and load at break

Sample	Cycles to Break	Load at Break	% Variation from Baseline
Uncoated	6th cycle	63236 N	2%
1 (2 – 4)	4th cycle	56393 N	13%
2 (2 – 8)	3rd cycle	51454 N	20%
3 (4 – 4)	4th cycle	56180 N	13%
4 (4 – 8)	3rd cycle	54690 N	15%

8-hour test results of Specimen 1 (2 – 4) are tabulated below in Figure 4.11, Figure 4.12 and Table 4.7:

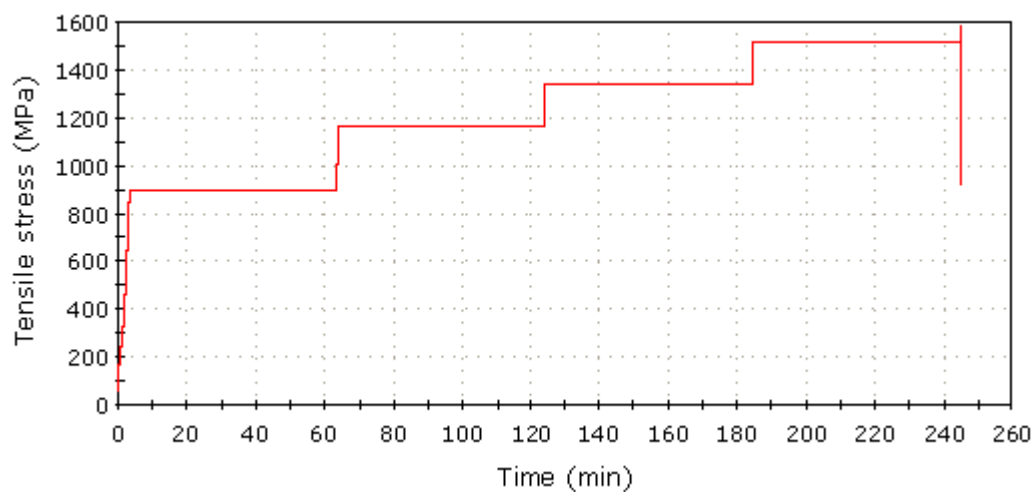


Figure 4.11. Time vs Tensile Stress graph of notched, round tensile specimen 1 (2 – 4), made of modified 4340 steel subjected to 8-hour test, break at 4th cycle

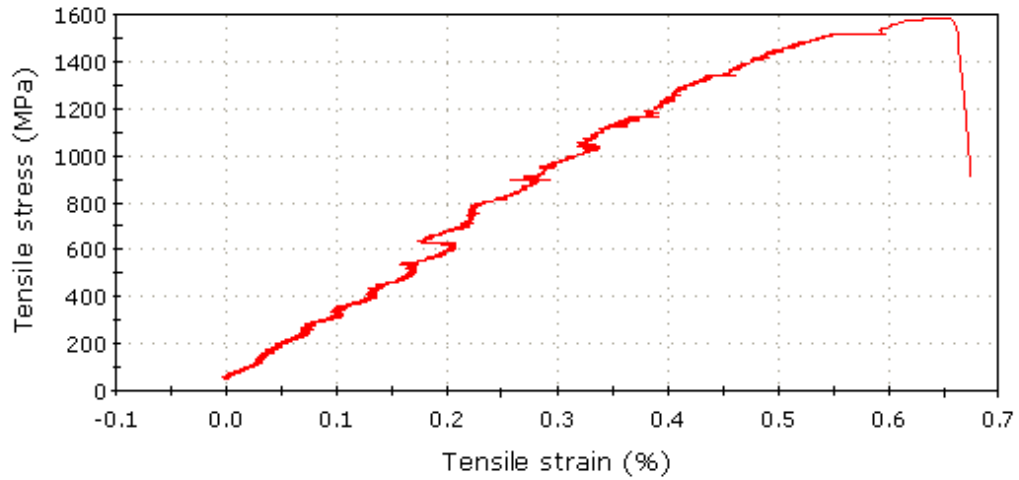


Figure 4.12. Stress vs Strain curve obtained from the 8-hour test of notched, round tensile specimen 1 (2 – 4)

Table 4.7. Mechanical data obtained from the 8-hour test of notched round specimen 1 (2 – 4)

<i>Axial Strain at Break</i> (%)	<i>Load at Break</i> (N)	<i>Tensile Stress at Break</i> (MPa)	<i>Maximum Tensile Stress</i> (MPa)
0.66054	56393	1561	1581

<i>Load at Max. Tensile Stress</i> (N)	<i>Axial Strain at Yield (2% offset)</i> (%)	<i>Tensile Stress at Yield (2% offset)</i> (MPa)
57100	0.66054	1493

8-hour test results of Specimen 2 (2 – 8) are tabulated below in Figure 4.13, Figure 4.14 and Table 4.8:

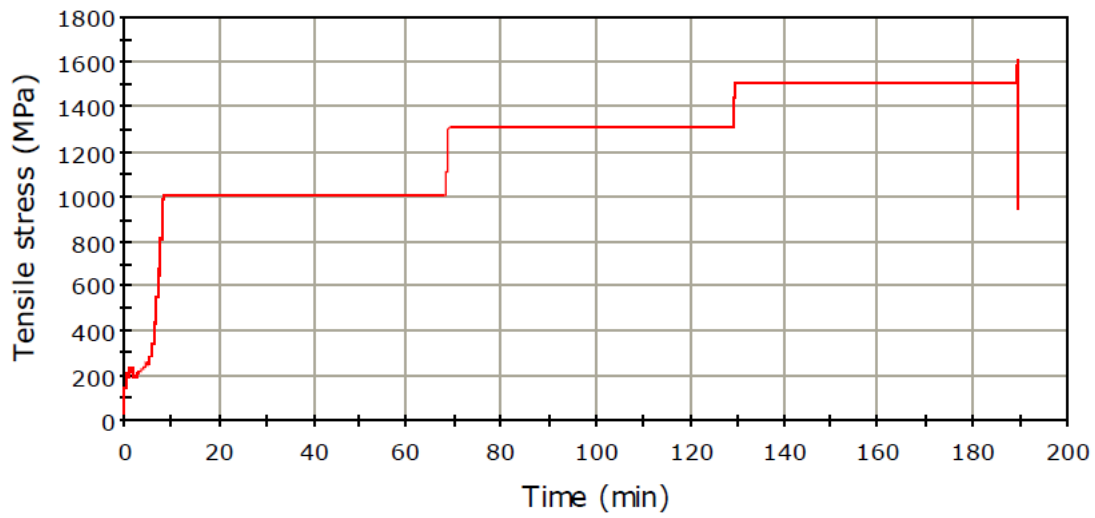


Figure 4.13. Time vs Tensile Stress graph of notched, round tensile specimen 2 (2 – 8), made of modified 4340 steel subjected to 8-hour test, break at 3rd cycle

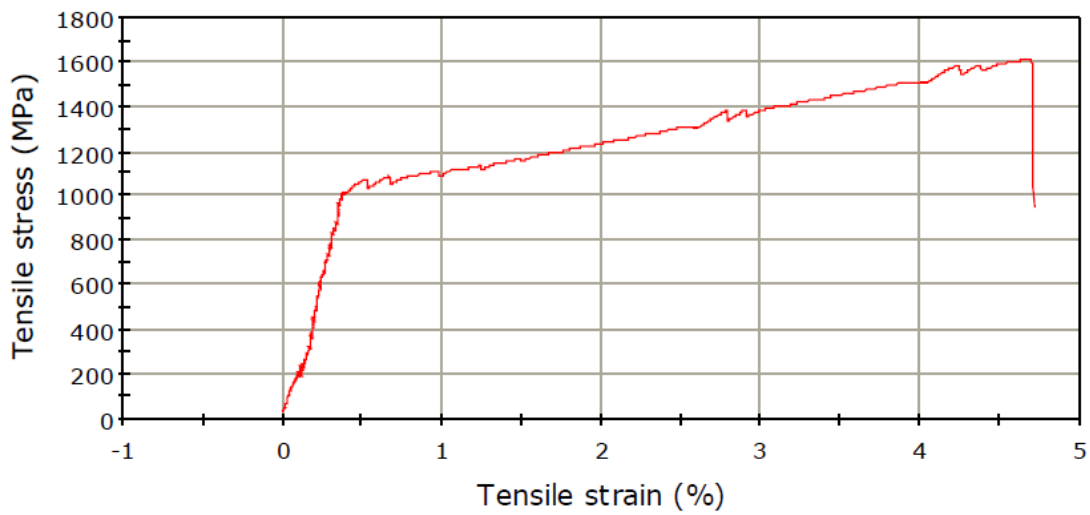


Figure 4.14. Stress vs Strain curve obtained from the 8-hour test of notched, round tensile specimen 2 (2 – 8)

Table 4.8. Mechanical data obtained from the 8-hour test of notched round specimen 2 (2 – 8)

<i>Axial Strain at Break (%)</i>	<i>Load at Break (N)</i>	<i>Tensile Stress at Break (MPa)</i>	<i>Maximum Tensile Stress (MPa)</i>
0.37694	51453	1604	1608

<i>Load at Max. Tensile Stress (N)</i>	<i>Axial Strain at Yield (2% offset) (%)</i>	<i>Tensile Stress at Yield (2% offset) (MPa)</i>
51578	0.37694	1048

8-hour test results of Specimen 3 (4 – 4) are tabulated below in Figure 4.15, Figure 4.16 and Table 4.9

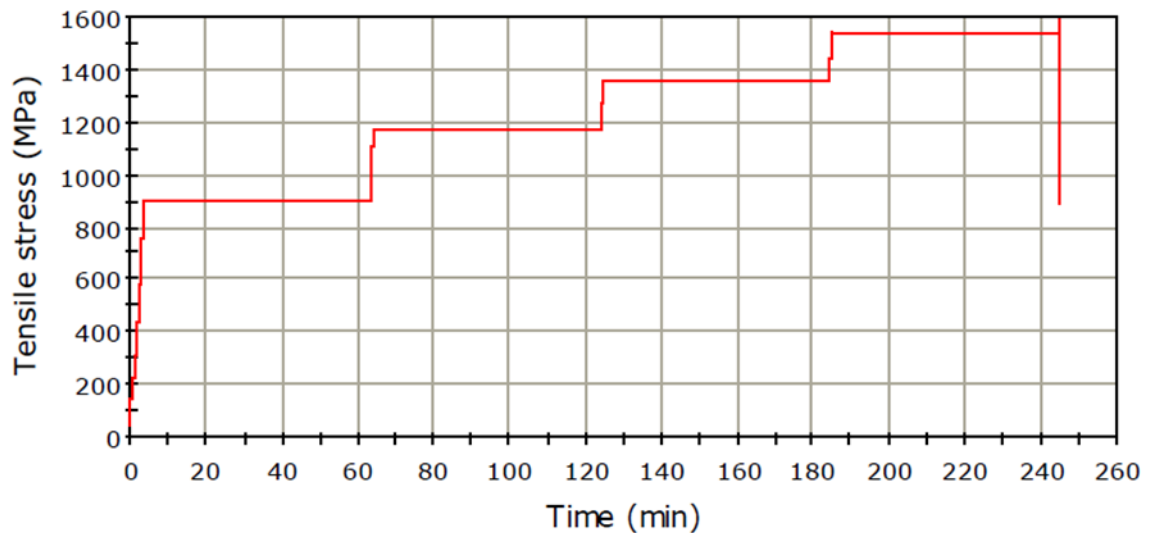


Figure 4.15. Time vs Tensile Stress graph of notched, round tensile specimen 3 (4 – 4), made of modified 4340 steel subjected to 8-hour test, break at 4th cycle

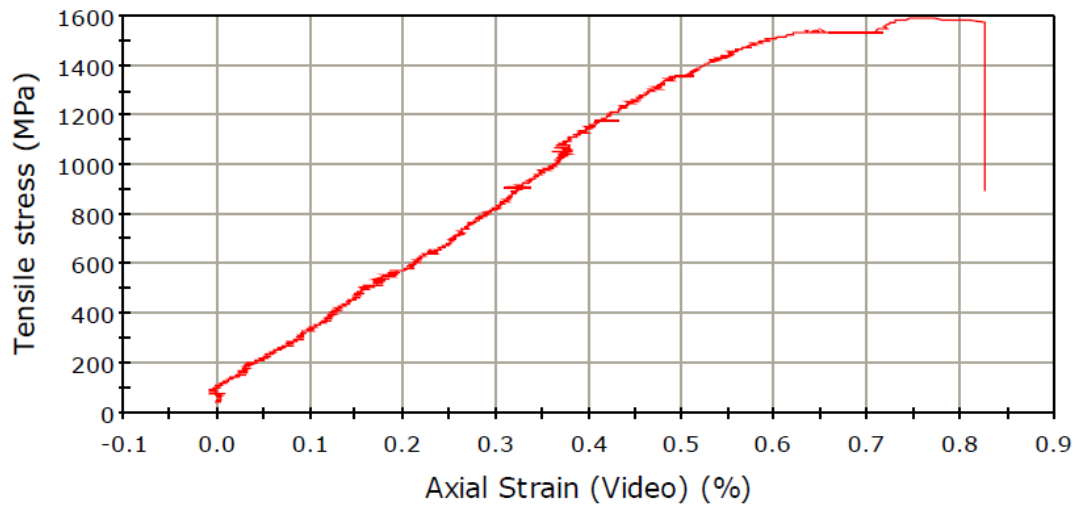


Figure 4.16. Stress vs Strain curve obtained from the 8-hour test of notched, round tensile specimen 3 (4 – 4)

Table 4.9. Mechanical data obtained from the 8-hour test of notched round specimen 3 (4 – 4)

<i>Axial Strain at Break (%)</i>	<i>Load at Break (N)</i>	<i>Tensile Stress at Break (MPa)</i>	<i>Maximum Tensile Stress (MPa)</i>
0.37694	51453	1604	1608

<i>Load at Max. Tensile Stress (N)</i>	<i>Axial Strain at Yield (2% offset) (%)</i>	<i>Tensile Stress at Yield (2% offset) (MPa)</i>
51578	0.37694	1048

8-hour test results of Specimen 4 (4 – 8) are tabulated below in Figure 4.17, Figure 4.18 and Table 4.10

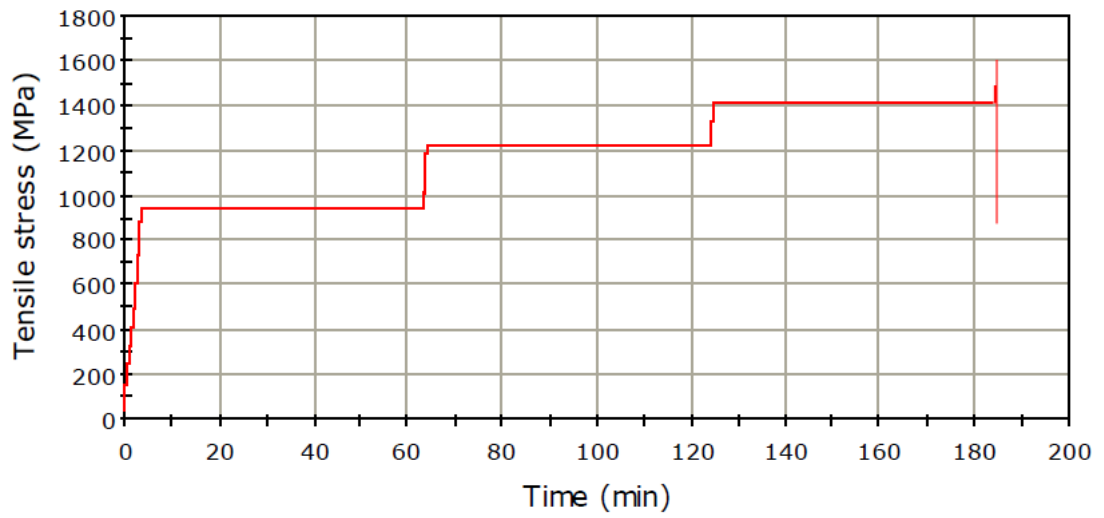


Figure 4.17. Time vs Tensile Stress graph of notched, round tensile specimen 4 (4 – 8), made of modified 4340 steel subjected to 8-hour test, break at 3rd cycle

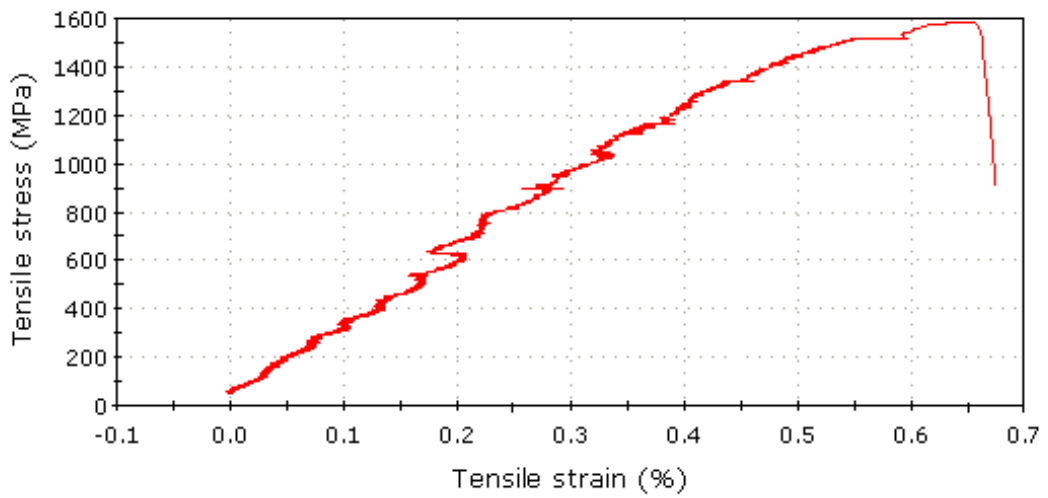


Figure 4.18. Stress vs Strain curve obtained from the 8-hour test of notched, round tensile specimen 4 (4 – 8)

Table 4.10. Mechanical data obtained from the 8-hour test of notched round specimen 4 (4 – 8)

<i>Axial Strain at Break</i> (%)	<i>Load at Break</i> (N)	<i>Tensile Stress at Break</i> (MPa)	<i>Maximum Tensile Stress</i> (MPa)
0.70757	54690	1598	1602

<i>Load at Max. Tensile Stress</i> (N)	<i>Axial Strain at Yield (2% offset)</i> (%)	<i>Tensile Stress at Yield (2% offset)</i> (MPa)
54822	0.70757	1305

Following you can see several SEM images representing the features of the fracture surfaces of the samples through Figure 4.19 to Figure 4.21

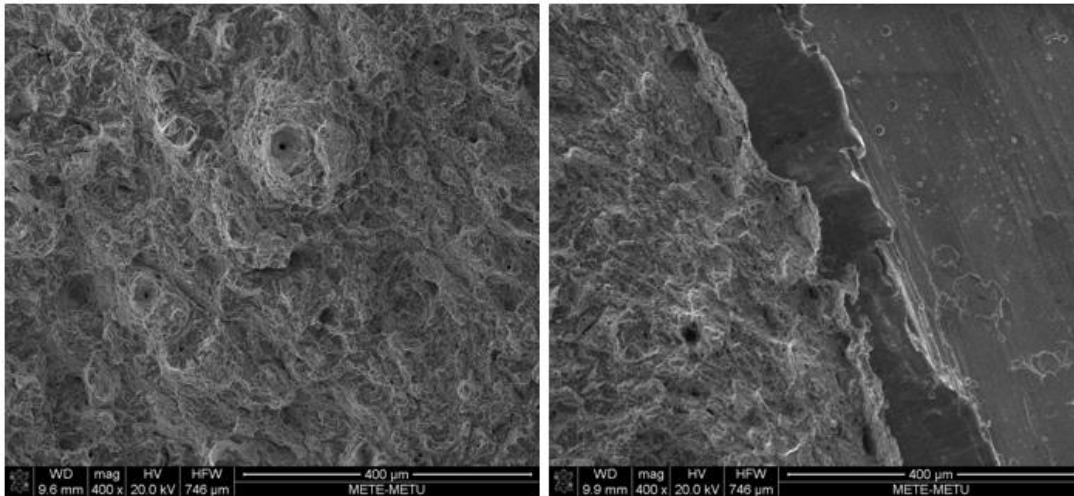


Figure 4.19. SEM image of the fracture surface of specimen 1 (2 – 4) subjected to 8-hour test taken from the core of the sample (on the left) modified 4340 steel and cadmium coating interface (on the right).

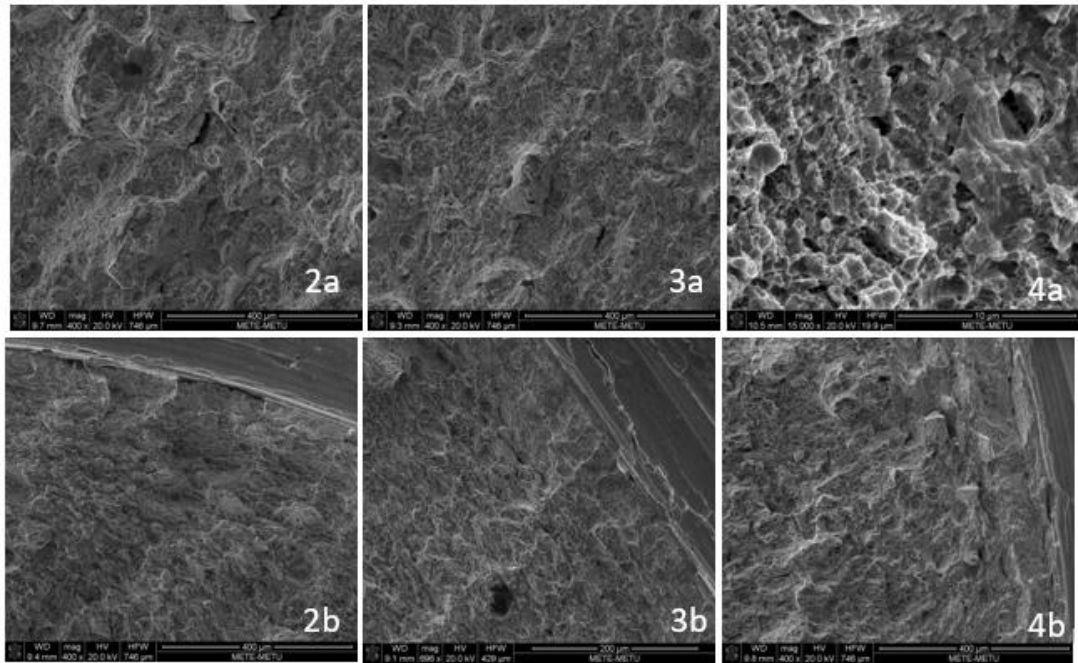


Figure 4.20. SEM image of the fracture surface of specimen 2 (2 – 8), 3 (4 – 4) and 4 (4 – 8), respectively, all after being subjected to 8-hour test. Photos are taken from (a) the core of the sample and (b) from the modified 4340 steel and cadmium coating interface

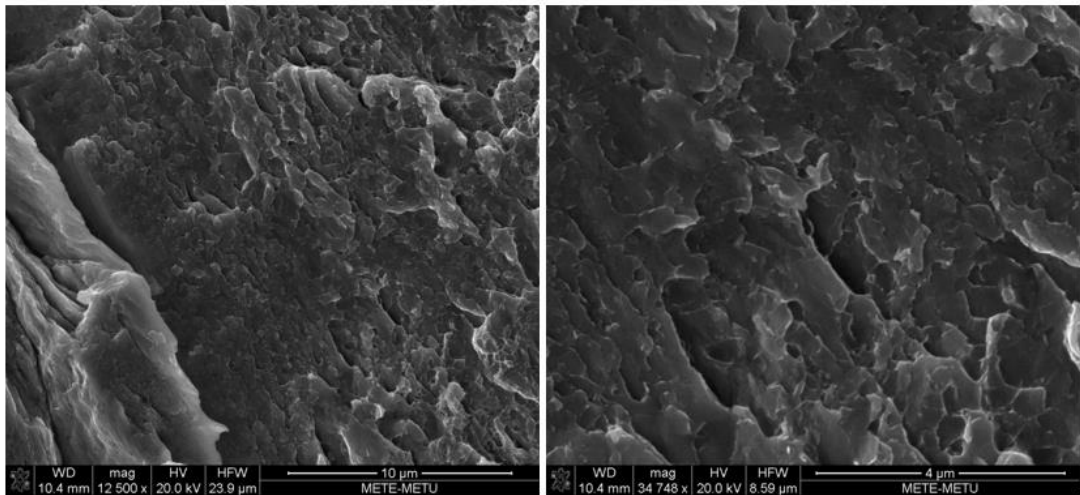


Figure 4.21. Some interesting features at fracture surface of 3rd specimen (4 – 4) located near the modified 4340 steel and cadmium coating interface

After the fractographic inspection of the fracture surfaces of samples subjected to 8-hour test, condition 1 (2 minutes of etching and 4 minutes of coating) being the least severe conditions were excluded and the fatigue tests were carried with the rest of the samples that were etched and coated using parameters given in Table 4.11 given below. This decision was based on the fact that although no coated sample could pass the 8-hour test successfully, all breaking at similar loads and during either cycle 3 or cycle 4. Sample 1 (2 – 4) withstand the highest load and based on the process parameters it was expected that it would possibly have less hydrogen absorbed in the structure.

4.6. Fatigue Test Results

35 hourglass specimens were used at rotating beam fatigue tests. Initially, 5 uncoated samples were tested at rotating beam testing machine to understand the behavior of modified 4340 steel before the application of cadmium coating. Rest of the samples were etched and coated under the conditions specified in Table 4.10. 10 identical samples of each set were used during fatigue tests. 15 samples composed of 3 different sets of samples were coated under the parameters given in Table 4.11 where each set consisted of 5 identical samples were fatigue tested in as coated condition and a preloading operation was introduced to a second batch of 15 samples coated under the same conditions after the analysis of the results of the initial tests.

Table 4.11. *Etching and coating conditions of the samples used for rotating beam fatigue testing*

SAMPLE	ETCH	COAT
1	Non - coated	
2 (2-8)	2 min	8 min
3 (4-4)	4 min	4 min
4 (4-8)	4 min	8 min

These specimens are tested with rotating beam testing machine under 5 different loads being 119 N, 140N, 170 N, 230 N and 350 N respectively.

S values are derived from the F values measured by load cell on the rotating beam testing machine using the following formula that originates from the moment diagram of hour glass sample according to its alignment in the setup:

$$S = 32 F \frac{L - X}{\pi d^3} \quad \text{Eqn. 3}$$

Where;

S is the required stress,

F is the applied force

L is the force arm length

d is the specimen diameter

x is the distance along the specimen axis from the fixed bearing face to the stress measurement plane

Although usually there is a direct correlation between tensile strength and fatigue strength; higher-tensile-strength steels are said to have higher endurance limits. Common exception is that the endurance limit is in the range of 35% to 60% of the tensile strength. ASM international suggests that this relationship would be valid up to a hardness of approximately 40 HRC (~1200 MPa, or 180 ksi tensile strength), and then the scatter becomes too great to be reliable. The measured hardness of modified 4340 steel used in this study corresponds to approximately 46 HRC which is greater than 40 HRC. As can be seen from the cycles to break data tabulated in Table 4.12 and 4.13 and respective graphics, the observed behavior suggests that the endurance limit is most likely around 384 MPa which correspond to approximately 30% of the measured UTS of modified 4340 steel. Where it comes to high strength steels it is important to note that the endurance limit is extremely sensitive to parameters residual-stress state, surface condition and the presence of inclusions that act as stress

concentrations and the metallographic examination of the samples cut from all 3 directions as can be seen in Figure 4.1 suggested that the base metal contained inclusions.

Table 4.12. *The cycles to break data obtained from the rotating beam fatigue testing of samples in as coated condition. (No preloading) UTS% is the corresponding percentage of ultimate tensile strength of modified 4340, S is the MPa value of UTS%, F is the applied load*

UTS (%)	S (MPa)	F (N)	# of cycles uncoated	# of cycles 4 etch / 8 coat	# of cycles 4 etch / 4 coat	# of cycles 2 etch / 8 coat
82.90	1127.14	350	8611	5401	6526	6097
54.48	740.70	230	48304	41542	38412	37133
40.28	547.48	170	73181	99140	148251	146582
33.16	450.86	140	252894	228794	231849	431424
28.18	383.22	119	658013	∞	383977	∞

S-N curves were plotted using the values tabulated in Table 4.12. The related S – N curves are given in Figure 4.22.

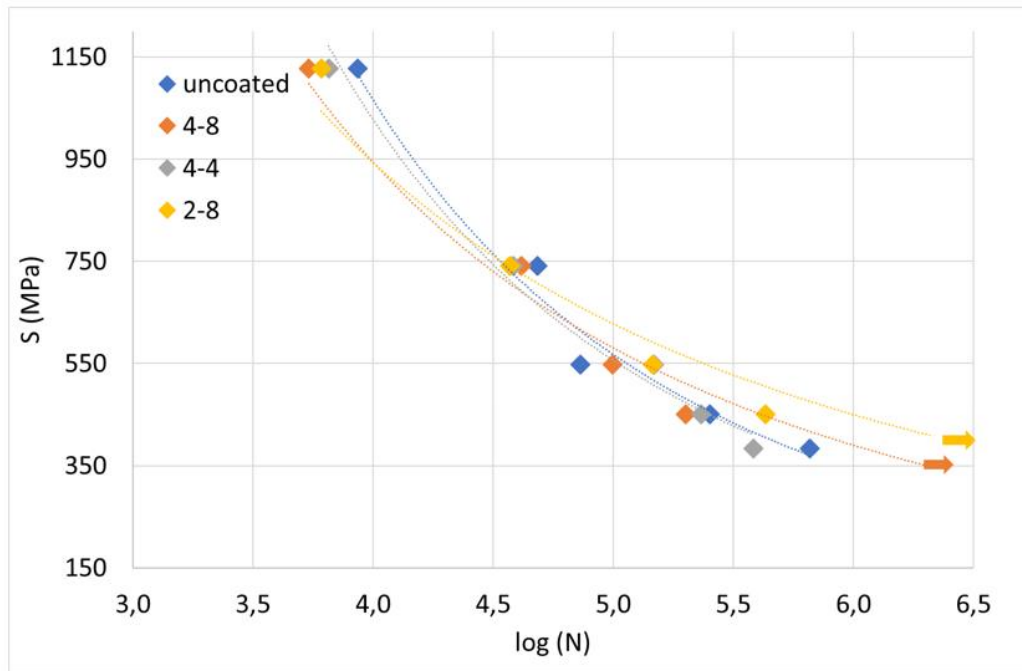


Figure 4.22. The semi log plot of S vs N for uncoated, 4 min etched 8 min coated (4 – 8), 4 min etched 4 min coated (4 – 4), 2 min etched 8 min coated (2 – 8) samples using data tabulated in Table 4.12

As seen in Figure 4.22, there appears to be no distinctive change in the fatigue life of uncoated and coated samples. All data lies within the same range and overlaps each other. However, it is important to note that below 600 MPa, the tendency of the data reveals that the material will reach its fatigue life limit. At high stress levels, the uncoated material has higher fatigue life than the coated ones. At low stress levels, the coated material has slightly higher fatigue life than the uncoated one.

In order to evaluate the effect of hydrogen, the samples were subjected to preload as described in the experimental section. The fatigue life was also measured after the preloading. Related data is tabulated in Table 4.13 and the S-N curves of the preloaded samples are given in Figure 4.23.

These preloaded specimens were also tested with rotating beam testing machine under the same loads used to test initial unloaded specimens.

Table 4.13. The cycles to break data obtained from the rotating beam fatigue testing of samples that are subjected to a preloading operation before the test. UTS% is the corresponding percentage of ultimate tensile strength of modified 4340, S is the MPa value of UTS%, F is the applied load

%UTS	S (MPa)	F (N)	# of cycles uncoated	# of cycles 4 etch / 8 coat	# of cycles 4 etch / 4 coat	# of cycles 2 etch / 8 coat
82.90	1127.14	350	8611	2733	3808	10849
54.48	740.70	230	48304	19701	25264	14040
40.28	547.48	170	73181	138452	87781	187289
33.16	450.86	140	252894	99746	113181	43627
28.18	383.22	119	658013	1465192	∞	267200

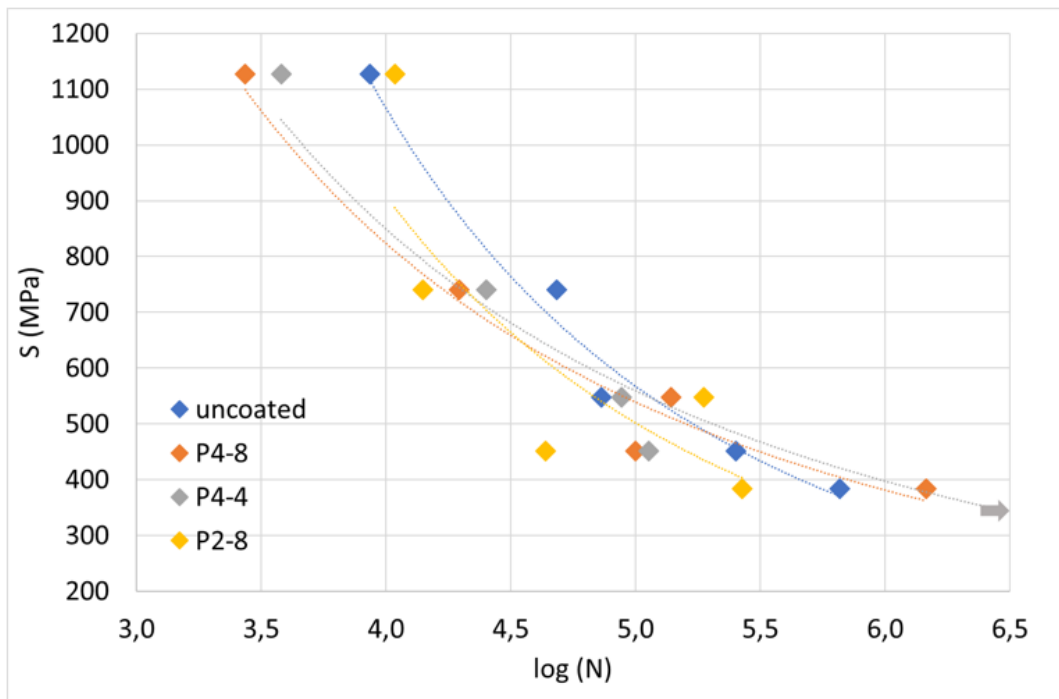


Figure 4.23. The semi log plot of S vs N for uncoated, preloaded samples of 4 min etched 8 min coated (P4 – 8) condition, preloaded samples of 4 min etched 4 min coated (P4 – 4) condition and samples of 2 min etched 8 min coated (2 – 8) condition using data tabulated in Table 4.13

The general trend of fatigue life of uncoated and preloaded samples appears to follow the similar S-N curve. Compared to the unloaded samples (as in Figure 4.22), the fatigue life of preloaded samples (as in Figure 4.23) has lower fatigue life than the uncoated and unloaded samples. Preloading has significant impact on the fatigue life. Therefore, it important to plot another set of graphs were the unloaded and preloaded fatigue lives of the samples coated using identical parameters were compared. This can be seen through Figure 4.24 to Figure 4.26

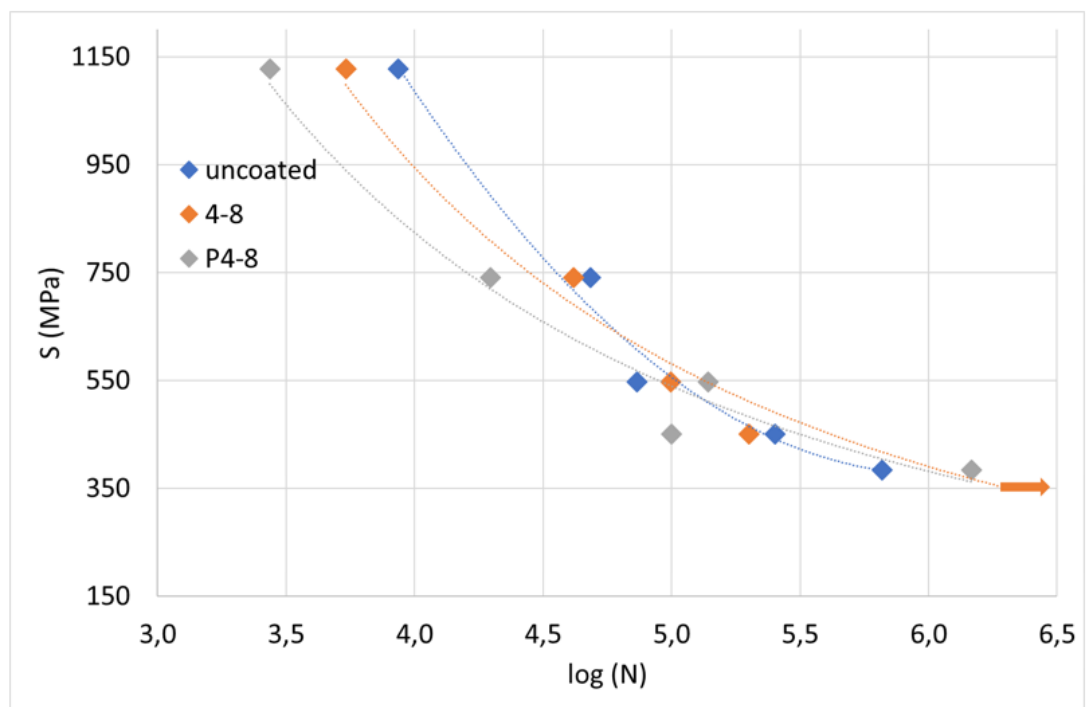


Figure 4.24. Comparison of S – N curves belonging to uncoated samples, unloaded (4 – 8) and preloaded (P4 – 8) samples of 4 min etching 8 min coating condition

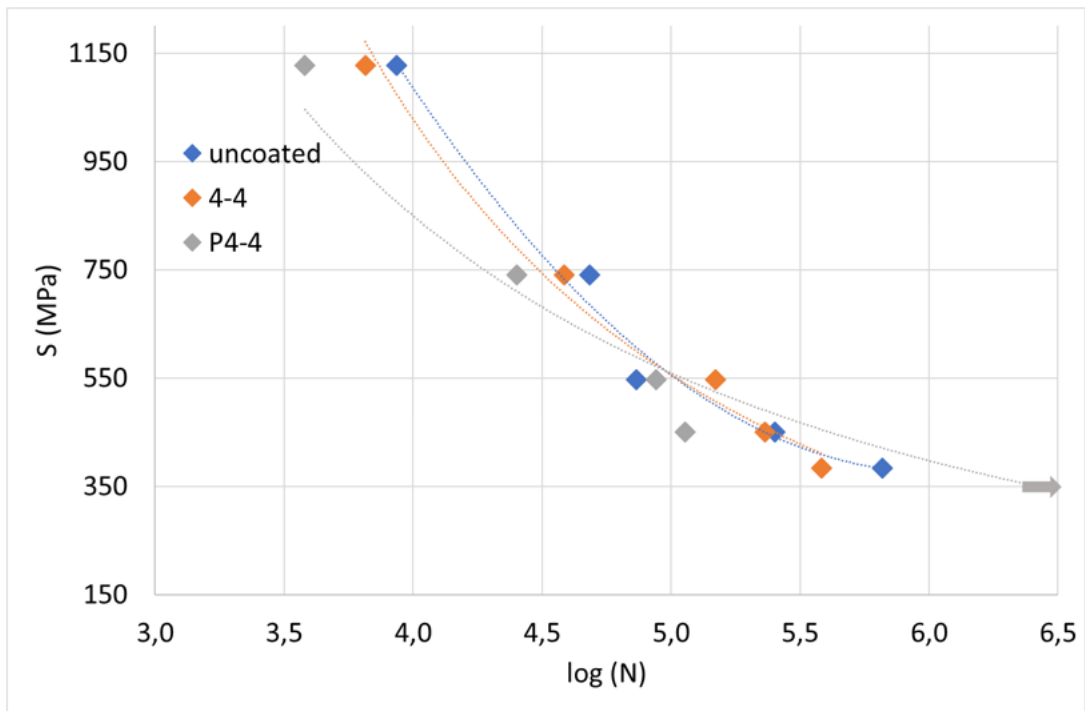


Figure 4.25. Comparison of S – N curves belonging to uncoated samples, unloaded (4 – 4) and preloaded (P4 – 4) samples of 4 min etching 4 min coating condition

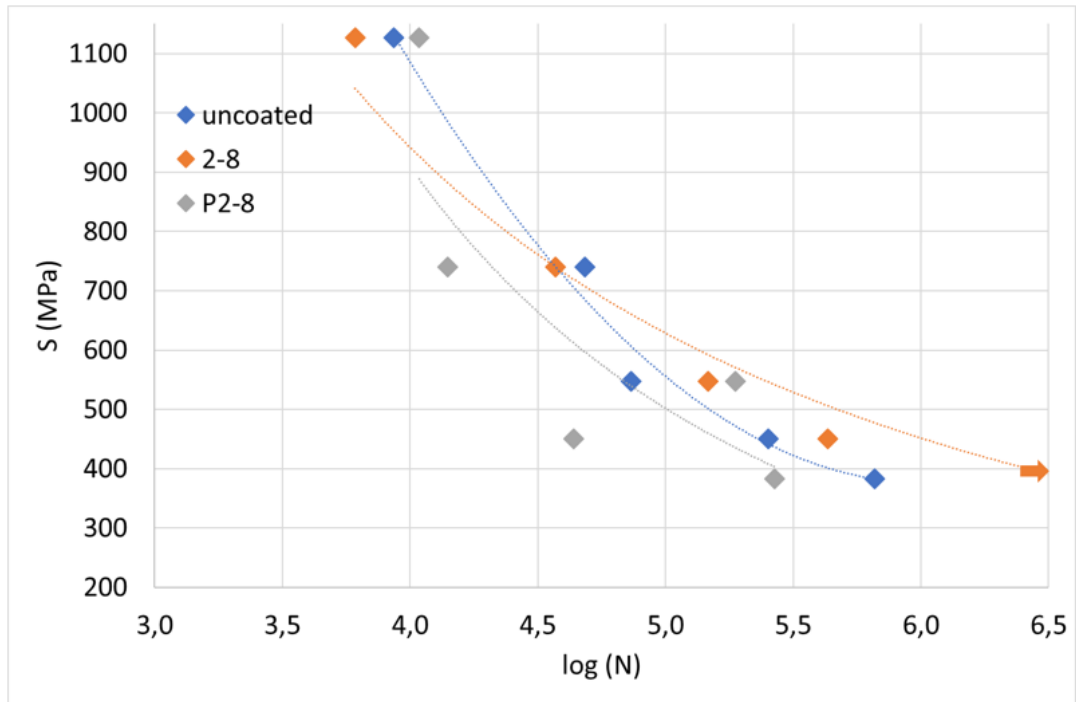


Figure 4.26. Comparison of S – N curves belonging to uncoated samples, unloaded (2 – 8) and preloaded (P2 – 8) samples of 2 min etching 8 min coating condition

Weibull statistics were applied to the fatigue life data and the results are given in Figure 4.27 and Figure 4.28 respectively.

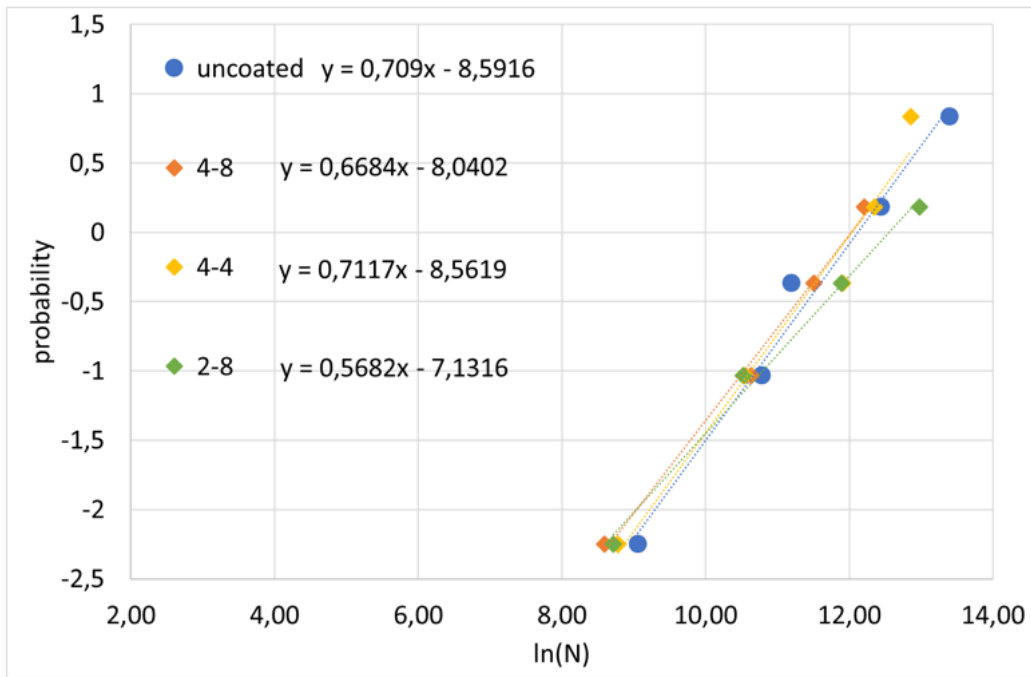


Figure 4.27. Weibull distribution of uncoated samples and samples without preloading

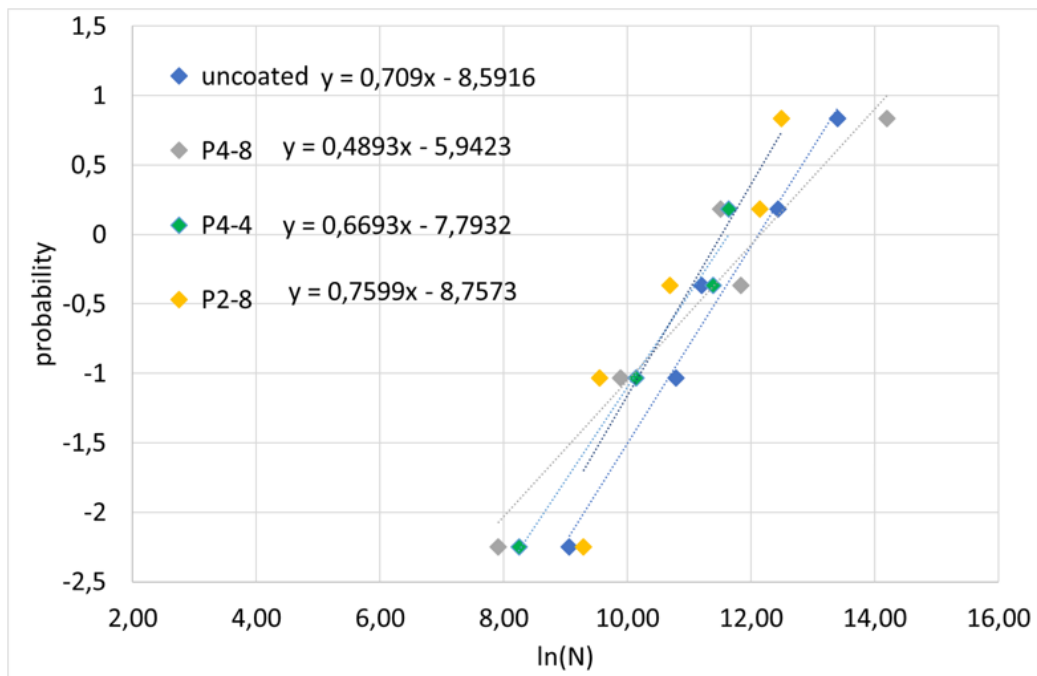


Figure 4.28. Weibull distribution of uncoated samples and samples with preloading

As can be seen in Weibull analysis, all data overlaps each other with a slight change in their reproducibility. The value that determines the repeatability is called Weibull modulus which is given in Table 4.14

Table 4.14. Weibull modulus of the rotating beam fatigue test results for each condition

Experimental condition	Weibull Modulus
uncoated	0.709
4-4	0.712
4-8	0.668
2-8	0.568
P4-4	0.669
P4-8	0.489
P2-8	0.759

A graphical representation of the Weibull modulus is given in Figure 4.29. It can be seen that the Weibull modulus of all the test results were between 0.4-0.8. P4-4 has the lowest reproducibility while P2-8 has the highest repeatability. On the other hand, it is important to compare the average scale parameter where P2-8 had the lowest value indicating that it was consistently bad.

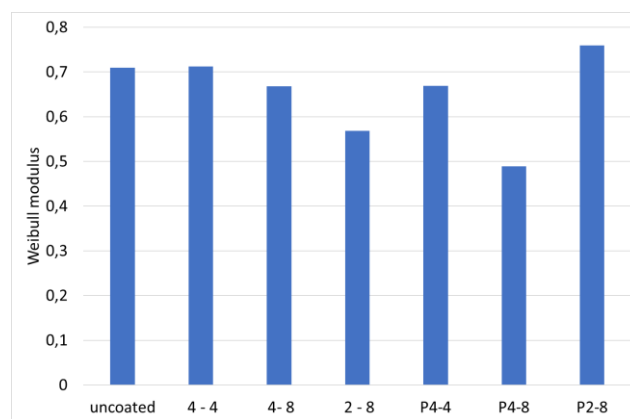


Figure 4.29. Graphical representation of Weibull modulus of $S - N$ data collected from all coating and loading conditions

Basquin slopes of the test conditions were calculated from the log/log plots as given in Figure 4.30 and Figure 4.31 respectively

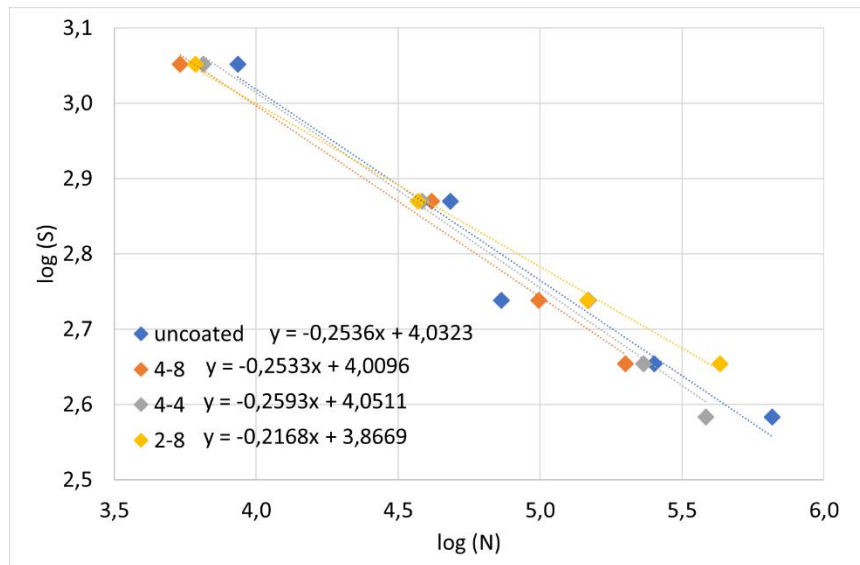


Figure 4.30. Graphical representation of the Basquin slope along with related equations for uncoated sample and unloaded samples

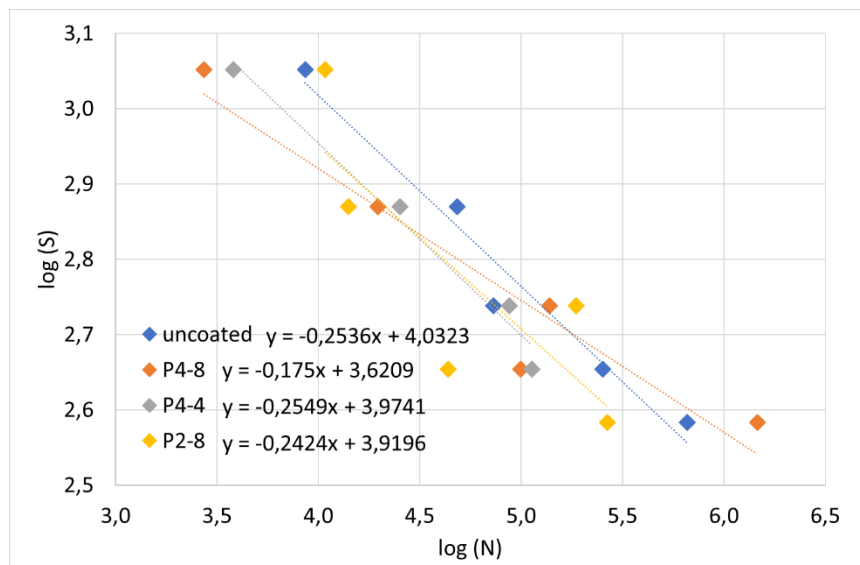


Figure 4.31. Graphical representation of the Basquin slope along with related equations for uncoated sample and preloaded samples

Below are the macro images and SEM images (from Figure 4.32 to Figure 4.49) of fracture surfaces of samples used to determine fatigue behavior. As can be seen from the given images fracture surfaces increase and fatigue surfaces decrease with increasing applied load. It is also observed that as the applied load increases possible crack initiation points also increase, at lower loads it is likely to determine a single point as the origin of the crack whereas fracture surfaces of the samples that were subjected to higher loads suggest multiple points of initiation.

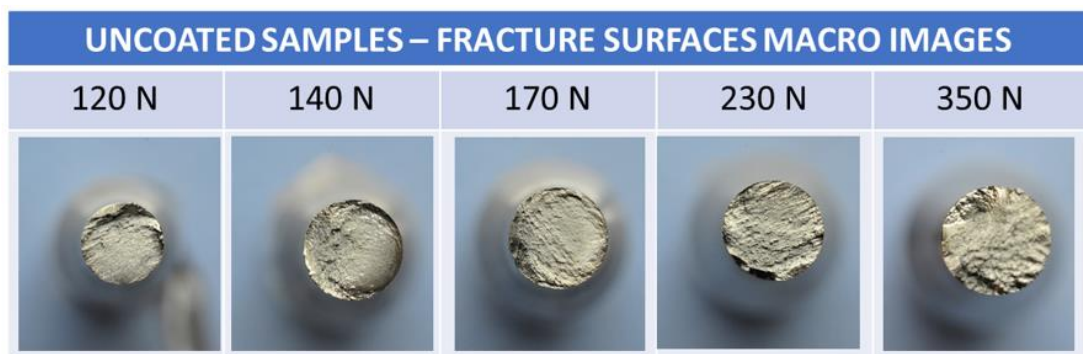


Figure 4.32. Macro images of the fracture surfaces of uncoated samples after the rotating beam fatigue test

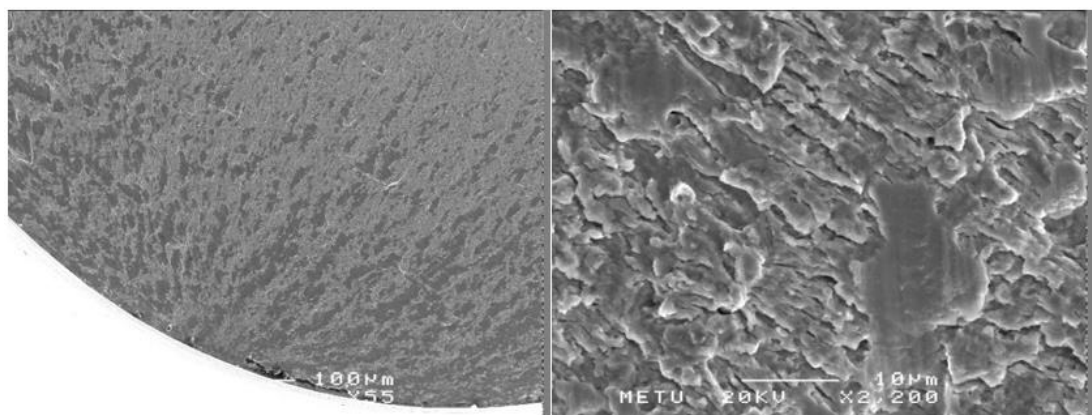


Figure 4.33. SEM images of possible crack initiation point and typical fatigue marks observed on the fracture surface of uncoated sample subjected to cyclic loading under 140 N.

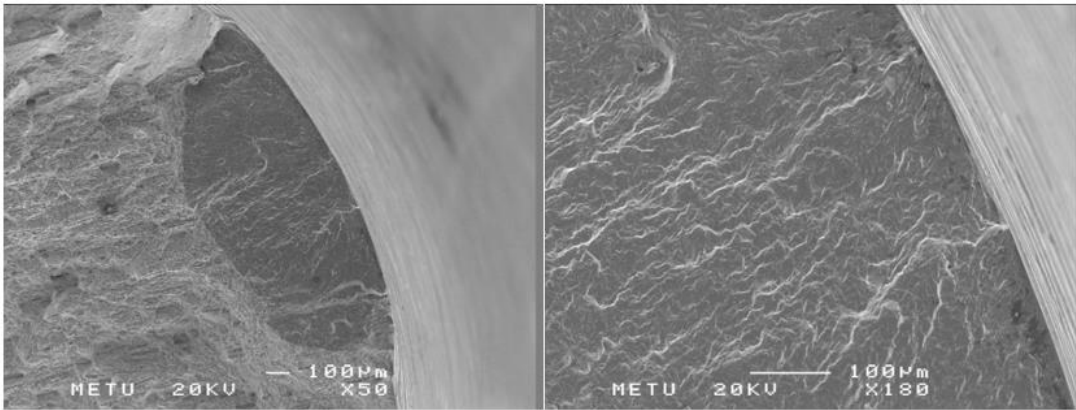


Figure 4.34. SEM images of possible crack initiation point and typical fatigue marks observed on the fracture surface of uncoated sample subjected to cyclic loading under 350 N.

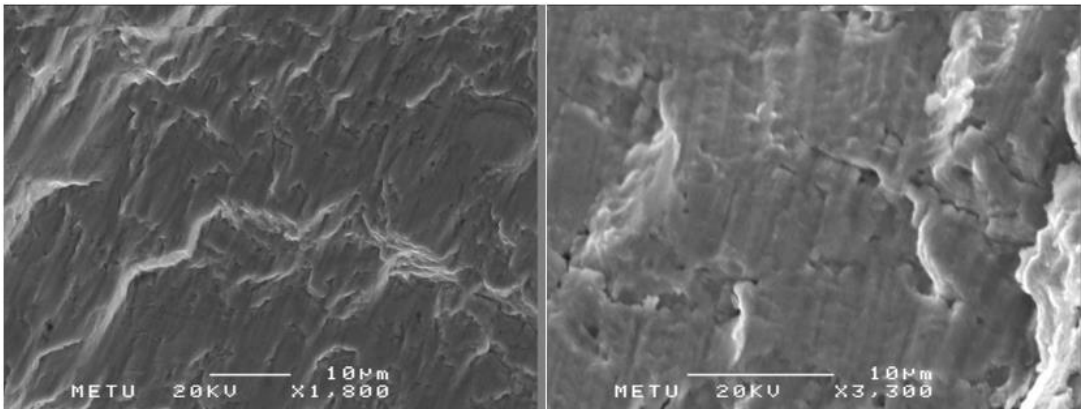


Figure 4.35. SEM images of a representative area where crack propagation can be observed on the fracture surface of uncoated sample subjected to cyclic loading under 350 N

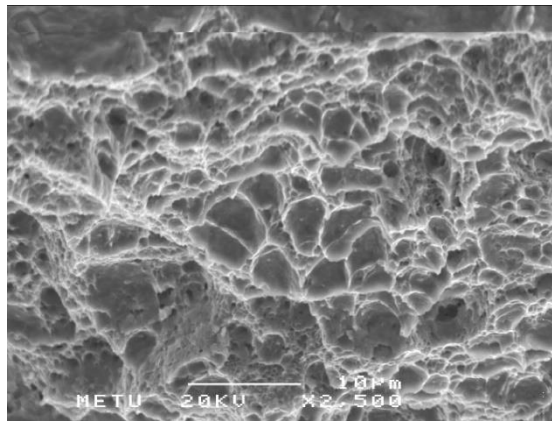


Figure 4.36. SEM image of fast fracture are ductile nature is observed on the fracture surface of uncoated sample subjected to cyclic loading under 350 N

UNLOADED SAMPLES – FRACTURE SURFACES MACRO IMAGES					
	120 N	140 N	170 N	230 N	350 N
4 min etched – 8 min coated					
4 min etched – 4 min coated					
2 min etched – 8 min coated					

Figure 4.37. Macro images of the fracture surfaces of the samples that were coated under given conditions after the rotating beam fatigue test. No load was introduced prior to fatigue testing

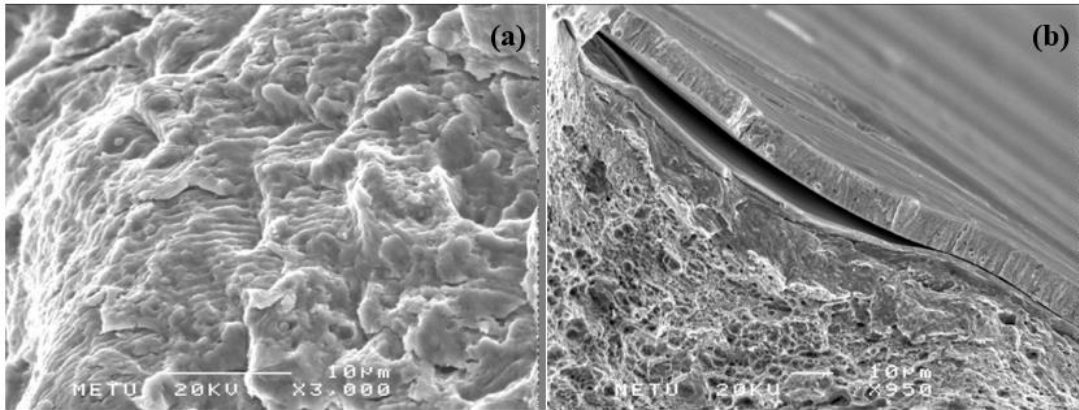


Figure 4.38. Image from the Sample (2 – 8) fractured under cyclic loading of 140 N showing (a) crack propagation at center and (b) possible fast fracture area at the edge

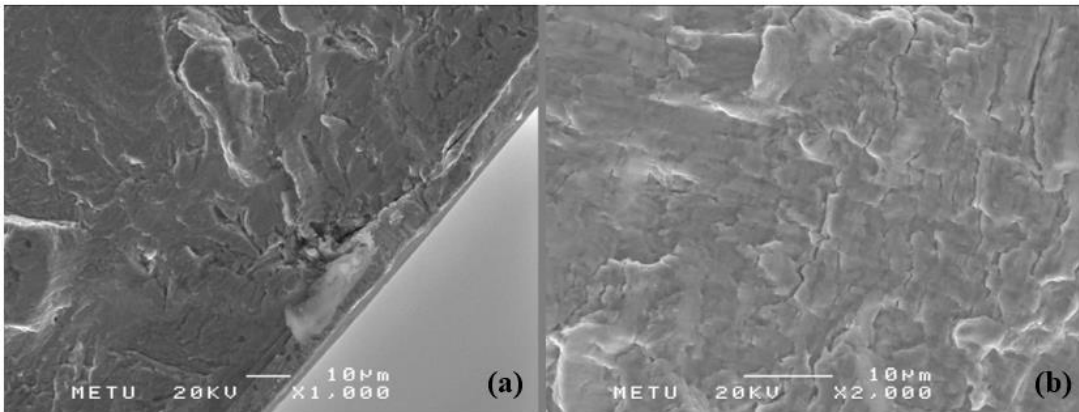


Figure 4.39. Image from the Sample (2 – 8) fractured under cyclic loading of 350 N showing (a) crack initiation and (b) crack propagation

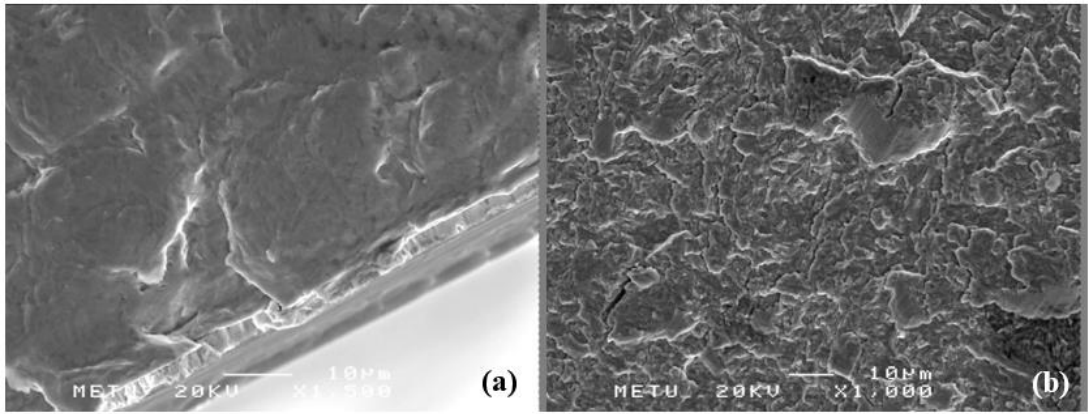


Figure 4.40. Image from Sample (4 – 4) fractured under cyclic loading of 140 N showing (a) crack initiation propagation and (b) crack propagation

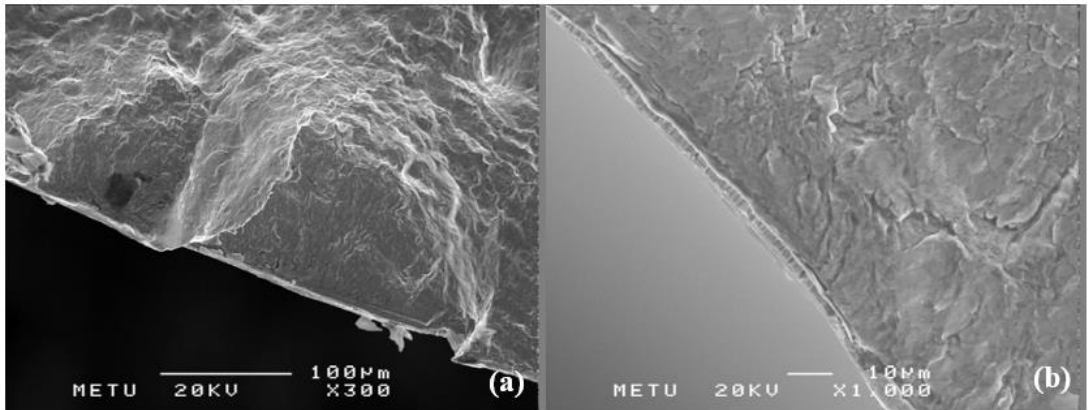


Figure 4.41. Image from Sample (4 – 4) fractured under cyclic loading of 350 N showing (a) small fatigue cracks and (b) representative fatigue area

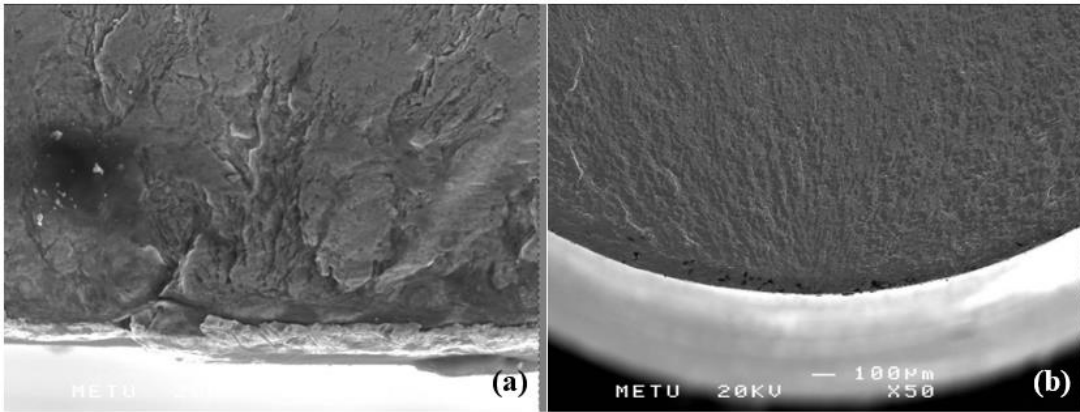


Figure 4.42. Image from the Sample (4 – 8) fractured under cyclic loading of 140 N showing (a) crack initiation and (b) crack propagation

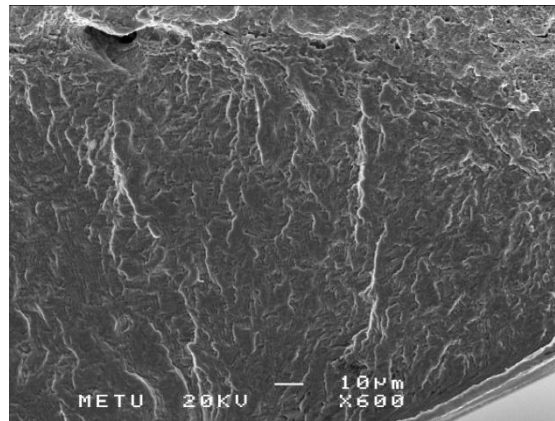


Figure 4.43. Image from the Sample (4 – 8) fractured under cyclic loading of 350 N showing river patterns at the fatigue surface

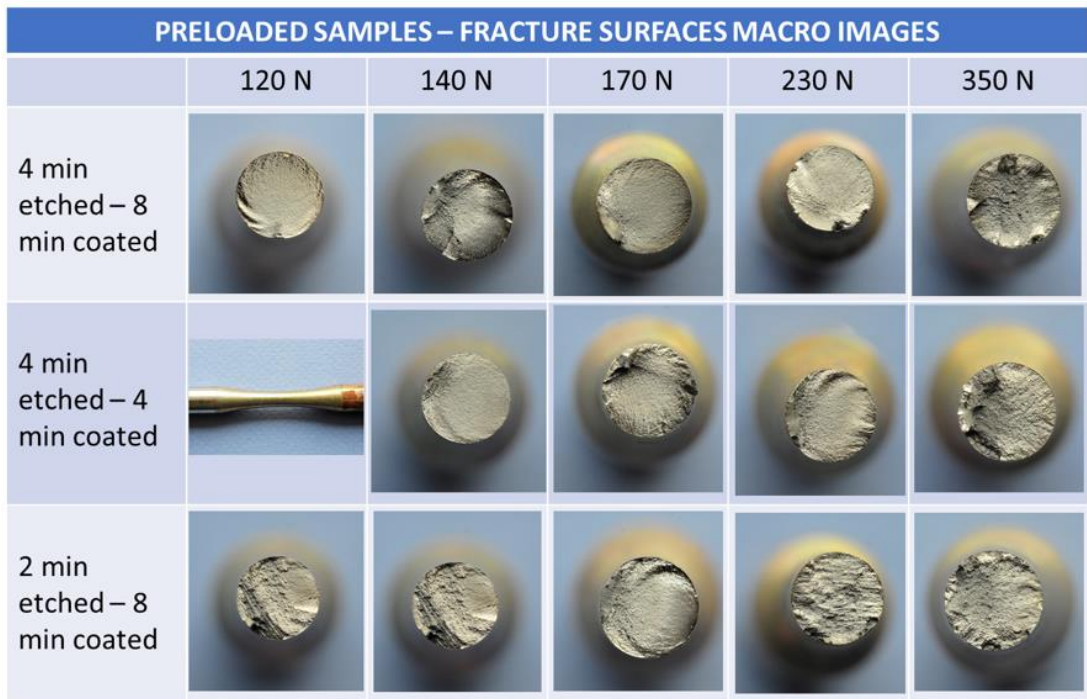


Figure 4.44. Macro images of the fracture surfaces of the samples that were coated under given conditions after the rotating beam fatigue test. The samples were preloaded prior to fatigue testing

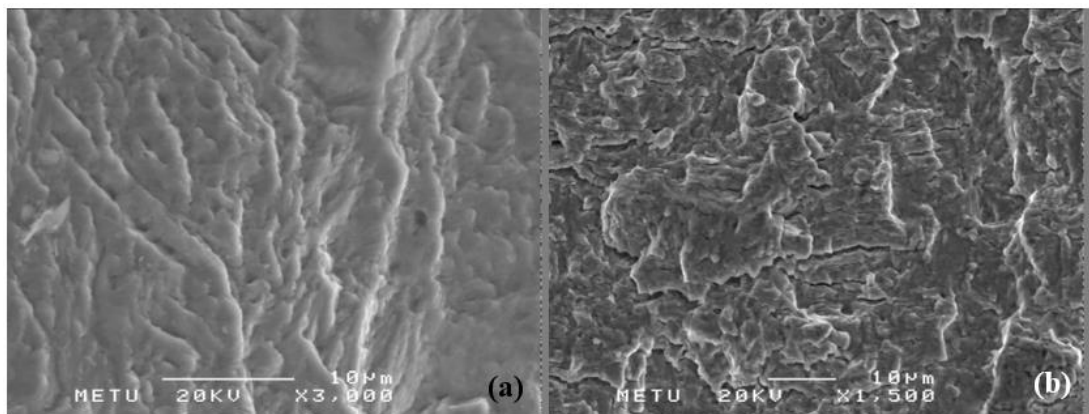


Figure 4.45. SEM images of possible crack propagation areas (a) close to edge and (b) from the centre observed on the fracture surface of preloaded sample (P2 – 8) subjected to cyclic loading under 140 N

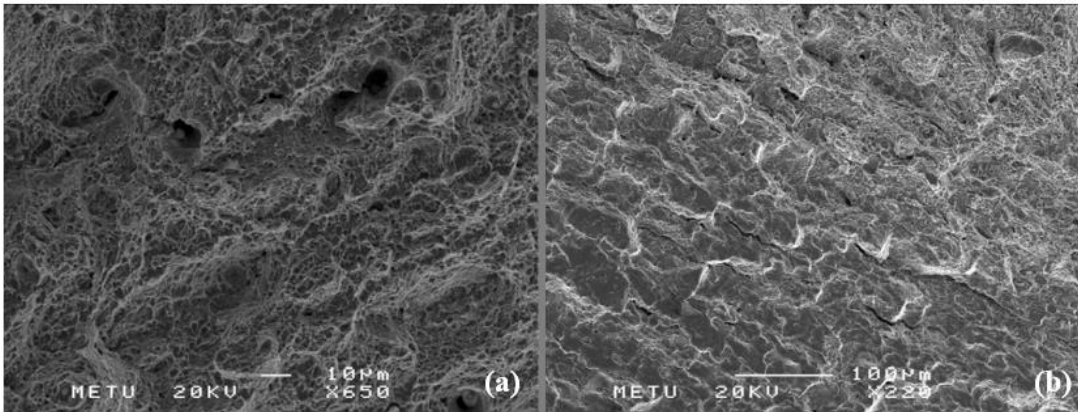


Figure 4.46. Image from the Sample (P2 – 8) fractured under cyclic loading of 350 N (a) sudden fracture area and (b) an area with intergranular fracture like appearance

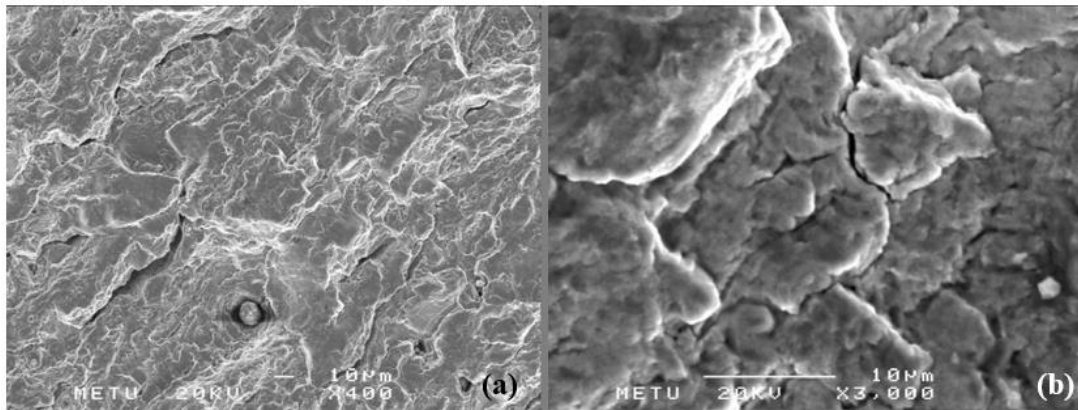


Figure 4.47. Image from the Sample (P4 – 4) fractured under cyclic loading of 350 N (a) sudden fracture area and (b) an area with intergranular fracture like appearance

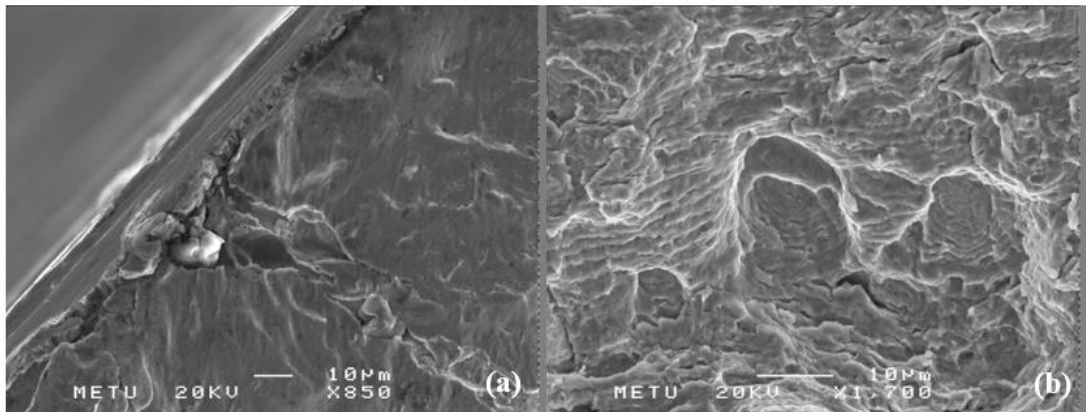


Figure 4.48. SEM images of (a) possible crack initiation point and (b) striation marks and crack propagation from the center observed on the fracture surface of preloaded sample (P4 – 8) subjected to cyclic loading under 140 N

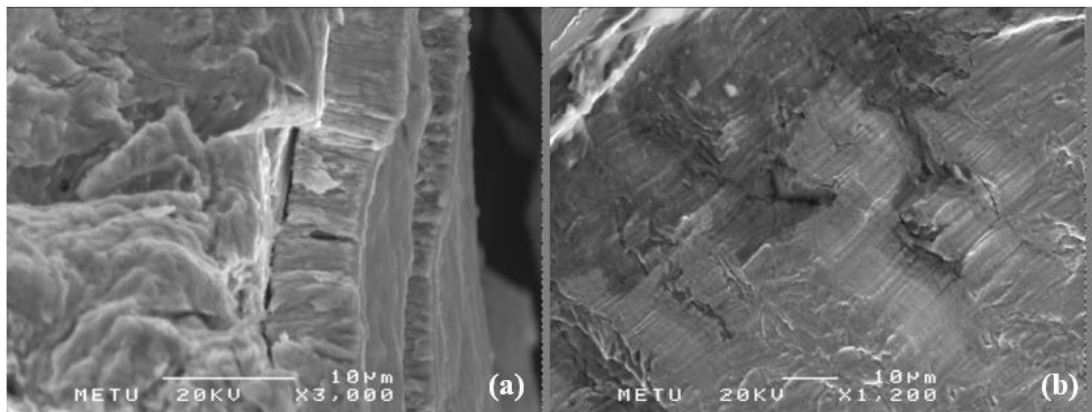


Figure 4.49. Image from the Sample (P4 – 8) fractured under cyclic loading of 350 N (a) close up of a fatigue crack and (b) typical propagation surface

CHAPTER 5

CONCLUSION

As coating duration was increased from 4 to 8 minutes, there is no significant increase in the coating thickness. There is approximately 2 μm change for both conditions.

Preloading of samples prior to fatigue test resulted in lowered fatigue life. This case is valid for all the fatigue stress above 600 MPa. When tests were carried out at 90 N (corresponding to 145 MPa or 11% UTS), no failure was observed. Thus, the experiments were conducted between loads of 120 N (corresponding to 383 MPa or 28% UTS) and 350 N (corresponding to 1127 MPa or 83% UTS). Beyond 350 N with the set up used, the hourglass sample would not withstand cyclic loading; premature failures were observed under 350 N of load. Beyond 350 N with the set up used, the hourglass sample would not withstand cyclic loading; premature failures were observed under 350 N of load.

Weibull statistics show that the test conditions studied in this work are consistent in terms of reproducibility and repeatability; minor changes of 0.27 max between modulus were identified.

All fatigue life data shows similar characteristics. There is a minor but repeated reduction in fatigue life of preloaded sample when compared with unloaded samples. This behavior is more apparent within the low cycle fatigue region.

According to the findings discussed above and the outcome of this work, it is recommended that future work is necessary to determine with more certainty and characterize the relationship between hydrogen contamination and fatigue life of Cadmium coated high strength steels

REFERENCES

- [1] B. P. Bardes, ASM Metals Handbook, 9th edition, Volume 1, 2019, pp. 124.
- [2] Azom, "SAE/AISI carbon steel naming conventions", July 2012, [Online] Available from: <https://www.azom.com> [Accessed 10 March 2019].
- [3] D. Figueroa and M. J. Robinson, "The effects of sacrificial coatings on hydrogen embrittlement and re-embrittlement of ultra high strength steels," *Corros. Sci.*, vol. 50, no. 4, pp. 1066–1079, 2008.
- [4] K. R. Sriraman, S. Brahim, J. A. Szpunar, and S. Yue, "Hydrogen embrittlement of Zn-, Zn-Ni-, and Cd-coated high strength steel," *J. Appl. Electrochem.*, vol. 43, no. 4, pp. 441–451, Apr. 2013.
- [5] V. Sabelkin, S. Mall, and H. Misak, "Corrosion fatigue of coated AISI 4340 high strength steel with dent damage," *Fatigue Fract. Eng. Mater. Struct.*, vol. 41, no. 3, pp. 653–662, 2018.
- [6] A. Conde, M. A. Arenas, and J. J. de Damborenea, "Electrodeposition of Zn-Ni coatings as Cd replacement for corrosion protection of high strength steel," *Corros. Sci.*, vol. 53, no. 4, pp. 1489–1497, 2011.
- [7] V. Sabelkin, H. Misak, and S. Mall, "Fatigue behavior of Zn-Ni and Cd coated AISI 4340 steel with scribed damage in saltwater environment," *Int. J. Fatigue*, vol. 90, pp. 158–165, 2016.
- [8] I. M. Robertson *et al.*, "Hydrogen Embrittlement Understood," *Metall. Mater. Trans. A*, vol. 46, no. 6, pp. 2323–2341, Jun. 2015.
- [9] M. Nagumo and K. Takai, "The predominant role of strain-induced vacancies in hydrogen embrittlement of steels: Overview," *Acta Mater.*, 2018.
- [10] J. Sanchez, S. F. Lee, M. A. Martin-Rengel, J. Fulla, C. Andrade, and J. Ruiz-Hervías, "Measurement of hydrogen and embrittlement of high strength steels," *Eng. Fail. Anal.*, vol. 59, pp. 467–477, 2016.
- [11] A. Nagao, M. Dadfarnia, P. Sofronis, and I. Robertson, "Hydrogen embrittlement: mechanisms," in *Encyclopedia of Iron, Steel, and Their Alloys (Online Version)*, CRC Press, 2016, pp. 1768–1784.
- [12] M. B. Djukic, V. S. Zeravic, G. M. Bakic, A. Sedmak, and B. Rajicic,

- “Hydrogen damage of steels: A case study and hydrogen embrittlement model,” *Eng. Fail. Anal.*, vol. 58, pp. 485–498, 2015.
- [13] H. K. D. H. Bhadeshia, “Prevention of hydrogen embrittlement in steels,” *ISIJ Int.*, vol. 56, no. 1, pp. 24–36, 2016.
- [14] D. H. Herring - *The Heat Treat Doctor*, “Hydrogen embrittlement”, 2006, [Online] Available from: <http://www.heat-treat-doctor.com> [Accessed 10 March 2019].
- [15] L. P. Pfeil, “No Title,” *Proc. R. Soc. London*, vol. 112, pp. 182–195, 1926.
- [16] Y. Murakami, T. Kanazaki, Y. Mine, and S. Matsuoka, “Hydrogen embrittlement mechanism in fatigue of austenitic stainless steels,” *Metall. Mater. Trans. A*, vol. 39, no. 6, p. 1327, 2008.
- [17] H. E. Boyer and A. S. Metals, *Atlas of Fatigue Curves*. American Society for Metals, 1985.
- [18] Total Materia, "Fatigue of Metals: Part Three", Aug 2010, [Online] Available from: <https://www.totalmateria.com/page.aspx?ID=CheckArticle&site=kts&NM=282> [Accessed 10 March 2019].
- [19] M. A. S. Torres and H. J. C. Voorwald, “An evaluation of shot peening, residual stress and stress relaxation on the fatigue life of AISI 4340 steel,” *Int. J. Fatigue*, vol. 24, no. 8, pp. 877–886, 2002.
- [20] J. Lankford and F. N. Kusenberger, “Initiation of fatigue cracks in 4340 steel,” *Metall. Trans.*, vol. 4, no. 2, pp. 553–559, 1973.
- [21] Y. Chew, J. H. L. Pang, G. Bi, and B. Song, “Effects of laser cladding on fatigue performance of AISI 4340 steel in the as-clad and machine treated conditions,” *J. Mater. Process. Technol.*, vol. 243, pp. 246–257, 2017.
- [22] S. Y. Sirin, “Effect of hot dip galvanizing on the fatigue behavior of hot rolled and ion nitrided AISI 4340 steel,” *Int. J. Fatigue*, vol. 123, pp. 1–9, 2019.
- [23] Y. Chew and J. H. L. Pang, “Fatigue life prediction model for laser clad AISI 4340 specimens with multiple surface cracks,” *Int. J. Fatigue*, vol. 87, pp. 235–244, 2016.
- [24] K. Dutta and K. D. Bharathi, “Effect of Prior Ratcheting Deformation on Low Cycle Fatigue Behaviour of AISI 4340 Steel,” in *Fracture, Fatigue and Wear*, 2018, pp. 759–767.

- [25] A. Rasti, M. H. Sadeghi, and S. S. Farshi, “An investigation into the effect of surface integrity on the fatigue failure of AISI 4340 steel in different drilling strategies,” *Eng. Fail. Anal.*, vol. 95, pp. 66–81, 2019.
- [26] K. Sadananda and A. K. Vasudevan, “Crack growth behavior of 4340 steel under corrosion and corrosion fatigue conditions,” *Corros. Rev.*, vol. 33, no. 6, pp. 335–349, 2015.
- [27] S. W. Song, J.-N. Kim, H. J. Seo, T. Lee, and C. S. Lee, “Effects of carbon content on the tensile and fatigue properties in hydrogen-charged Fe-17Mn-xC steels: The opposing trends,” *Mater. Sci. Eng. A*, vol. 724, pp. 469–476, 2018.
- [28] H. Matsunaga, M. Yoshikawa, R. Kondo, J. Yamabe, and S. Matsuoka, “Slow strain rate tensile and fatigue properties of Cr–Mo and carbon steels in a 115 MPa hydrogen gas atmosphere,” *Int. J. Hydrogen Energy*, vol. 40, no. 16, pp. 5739–5748, 2015.
- [29] S. Wang, K. E. Nygren, A. Nagao, P. Sofronis, and I. M. Robertson, “On the failure of surface damage to assess the hydrogen-enhanced deformation ahead of crack tip in a cyclically loaded austenitic stainless steel,” *Scr. Mater.*, vol. 166, pp. 102–106, 2019.
- [30] I. M. Dmytrakh, R. L. Leshchak, A. M. Syrotyuk, and R. A. Barna, “Effect of hydrogen concentration on fatigue crack growth behaviour in pipeline steel,” *Int. J. Hydrogen Energy*, vol. 42, no. 9, pp. 6401–6408, 2017.
- [31] T. An, H. Peng, P. Bai, S. Zheng, X. Wen, and L. Zhang, “Influence of hydrogen pressure on fatigue properties of X80 pipeline steel,” *Int. J. Hydrogen Energy*, vol. 42, no. 23, pp. 15669–15678, 2017.
- [32] A. Nagao, S. Wang, K. E. Nygren, M. Dadfarnia, P. Sofronis, and I. M. Robertson, “Microstructural Change of Low Carbon and Low-Alloy Steels Caused by Hydrogen-Induced Fatigue-Crack Growth,” in *International Hydrogen Conference (IHC 2016): Materials Performance in Hydrogen Environments*, 2017.
- [33] A. Cheng and N.-Z. Chen, “Fatigue crack growth modelling for pipeline carbon steels under gaseous hydrogen conditions,” *Int. J. Fatigue*, vol. 96, pp. 152–161, 2017.
- [34] J. A. Ronevich, B. P. Somerday, and C. W. San Marchi, “Effects of microstructure banding on hydrogen assisted fatigue crack growth in X65 pipeline steels,” *Int. J. Fatigue*, vol. 82, pp. 497–504, 2016.

- [35] C. Colombo, G. Fumagalli, F. Bolzoni, G. Gobbi, and L. Vergani, “Fatigue behavior of hydrogen pre-charged low alloy Cr–Mo steel,” *Int. J. Fatigue*, vol. 83, pp. 2–9, 2016.
- [36] J. Yamabe, M. Yoshikawa, H. Matsunaga, and S. Matsuoka, “Effects of hydrogen pressure, test frequency and test temperature on fatigue crack growth properties of low-carbon steel in gaseous hydrogen,” *Procedia Struct. Integr.*, vol. 2, pp. 525–532, 2016.
- [37] Y. Ogawa *et al.*, “Multi-scale observation of hydrogen-induced, localized plastic deformation in fatigue-crack propagation in a pure iron,” *Scr. Mater.*, vol. 140, pp. 13–17, 2017.
- [38] Y. Ogawa, H. Matsunaga, J. Yamabe, M. Yoshikawa, and S. Matsuoka, “Unified evaluation of hydrogen-induced crack growth in fatigue tests and fracture toughness tests of a carbon steel,” *Int. J. Fatigue*, vol. 103, pp. 223–233, 2017.
- [39] R. L. Amaro, E. S. Drexler, N. Rustagi, N. E. Nanninga, Y. S. Levy, and A. J. Slifka, “Fatigue crack growth of pipeline steels in gaseous hydrogen-predictive model calibrated to API-5L X52,” in *International Hydrogen Conference, Moran, WY, Sept, 2012*, pp. 9–12.
- [40] A. D. Richardson, M.-H. Evans, L. Wang, R. J. K. Wood, and M. Ingram, “Thermal desorption analysis of hydrogen in non-hydrogen-charged rolling contact fatigue-tested 100Cr6 steel,” *Tribol. Lett.*, vol. 66, no. 1, p. 4, 2018.
- [41] R. P. Gangloff, “Hydrogen assisted cracking of high strength alloys”, *Comprehensive Structural Integrity*, Vol. 6, New York: Elsevier Science, 2003.